2018-02-01

Complementary biomarker-based methods for characterising Arctic sea ice conditions: A case study comparison between multivariate analysis and the PIP<inf>25</inf>index

Koseoglu, D

10.1016/j.gca.2017.11.001
Geochimica et Cosmochimica Acta
Elsevier BV

Complementary biomarker-based methods for characterising Arctic sea ice conditions: A case study comparison between multivariate analysis and the PIP_{25} index

Denizcan Köseoğlu[a], Simon T Belt[a,*], Lukas Smik[a], Haoyi Yao[b], Giuliana Panieri[b], Jochen Knies[b,c]

(a) Biogeochemistry Research Centre, School of Geography, Earth and Environmental Sciences, Plymouth University, Plymouth, PL4 8AA, UK.

(b) CAGE – Centre for Arctic Gas Hydrate, Environment and Climate, Department of Geosciences, UiT The Arctic University of Norway, 9037 Tromsø, Norway.

(c) Geological Survey of Norway, N-7491 Trondheim, Norway.

* Author for correspondence

E-mail: sbelt@plymouth.ac.uk

Keywords: Arctic; IP_{25}; Sea ice; Biomarker; HBI; Classification Tree; PIP_{25}

Abstract

The discovery of IP_{25} as a qualitative biomarker proxy for Arctic sea ice and subsequent introduction of the so-called PIP_{25} index for semi-quantitative descriptions of sea ice conditions has significantly advanced our understanding of long-term paleo Arctic sea ice conditions over the past decade. We investigated the potential for classification tree[1] (CT) models to provide a further approach to paleo Arctic sea ice reconstruction through analysis of a suite of highly branched isoprenoid (HBI) biomarkers in ca. 200 surface sediments from the Barents Sea. Four CT models constructed using different HBI assemblages revealed IP_{25} and an HBI triene as the most appropriate classifiers of sea ice conditions, achieving a >90% cross-validated classification rate. Additionally, lower model performance for locations in the Marginal Ice Zone (MIZ) highlighted difficulties in characterisation of this climatically-sensitive region. CT model classification and semi-quantitative PIP_{25}-derived estimates of spring sea ice concentration (SpSIC) for four downcore records from the region were consistent, although agreement between proxy and satellite/observational records was weaker for a core from the west Svalbard margin, likely due to the highly variable sea conditions. The automatic selection of appropriate biomarkers for description of sea ice conditions, quantitative model assessment, and insensitivity to the *c*-factor used in the calculation of the PIP_{25} index are key attributes of the CT approach, and we provide an initial comparative assessment between these potentially complementary methods. The CT model should be capable of generating longer-term temporal shifts in sea ice conditions for the climatically sensitive Barents Sea.

[1] Non-standard abbreviations:
CT – Classification tree

1. Introduction

Arctic sea ice is an important regulator of the ocean-atmosphere heat, gas and moisture fluxes (Smedsrud et al., 2013) and serves as an expansive habitat for a diverse ecosystem (Derocher et al., 2011; Vancoppenolle et al., 2013). Further, sea ice reflects up to 85% of incoming solar shortwave radiation (Perovich and Polashenski, 2012). The complex system of physical and thermodynamic interactions with the ocean and the atmosphere control the physical properties of sea ice, making it a sensitive indicator of global climate (Perovich and Richter-Menge, 2009; Meier et al., 2014, and references therein). During formation, sea ice expels brine, resulting in oceanic convection that facilitates formation of North Atlantic Deep Water (Bitz et al., 2006). In contrast, ice melt induces freshening and stratification of the upper water column, which limits convection and facilitates the development of primary productivity blooms, which occur along the receding sea ice edge, frequently referred to as the Marginal Ice Zone (MIZ; Wassmann et al., 1999).

The introduction of satellite-mounted passive microwave sensors has allowed regular monitoring of Arctic sea ice since the late 1970’s (e.g. Fetterer et al., 2016). The recent decline in Arctic sea ice extent (Stroeve et al., 2012) is unprecedented within the instrumental record (Divine and Dick, 2006; Walsh et al., 2017) and is thought to be influenced by anthropogenic warming (Hansen et al., 2010; Kinnard et al., 2011) and amplified by positive feedback mechanisms (Perovich and Polashenski, 2012). To better understand and predict modern sea ice trends, however, it is important to reconstruct longer-term sea ice variability throughout geological time using proxy measurements (de Vernal et al., 2013).

Recently, a C_{25} Highly Branched Isoprenoid (HBI) alkene, labelled IP_{25} (Ice Proxy with 25 carbon atoms; Belt et al., 2007), has been shown to be a suitable biomarker proxy of Arctic seasonal sea ice (Belt and Müller, 2013). The selectivity of IP_{25} towards seasonal sea ice cover is supported by its ^{13}C isotopic signature (Belt et al., 2008) and production by certain sympagic diatoms (e.g. *Haslea* and *Pleurosigma* spp.; Brown et al., 2014b) during the spring primary productivity bloom (Brown et al., 2011, 2014b; Belt et al., 2013). Further, investigations of IP_{25} in pan-Arctic surface sediments have revealed a consistent presence, primarily at seasonally ice-covered locations (Méheust et al., 2013; Stoynova et al., 2013; Weckström et al., 2013; Xiao et al., 2013, 2015a; Belt et al., 2015; Ribeiro et al., 2017). Within paleo records, IP_{25} has been identified in downcore records from all Arctic regions spanning a range of timeframes extending back to the late Miocene (e.g. Massé et al., 2008; Müller et al., 2009, 2012; Vare et al., 2009, 2010; Cabedo-Sanz et al., 2013; Knies et al., 2014, 2017; Müller and Stein, 2014; Cabedo-Sanz and Belt, 2016; Hoff et al., 2016; Polyak et al., 2016; Stein et al., 2016, 2017; Berben et al., 2017; Hörner et al., 2017).

A limitation of sea ice reconstructions based on sedimentary IP_{25} alone is the difficulty in distinguishing between perennial sea ice cover and ice-free conditions, as it is usually absent in both scenarios (Belt and Müller, 2013). However, it has been reported in sediments from regions of near-permanent sea ice cover (Xiao et al., 2015a). To address this possible ambiguity, Müller et al. (2009) first proposed concurrent analysis of certain phytoplankton biomarkers (e.g. brassicasterol) that are characteristic of open water (pelagic) conditions (Volkman, 1986, 2006). Subsequently, the combining of phytoplankton biomarker and IP_{25} concentrations to calculate a Phytoplankton–IP_{25} index (PIP_{25}) was used to obtain semi-quantitative descriptions of sea ice conditions (Müller et al., 2011). Sterol-based PIP_{25} indices

have since been utilised in several studies of both surface and downcore sedimentary records (e.g. Fahl and Stein, 2012; Müller et al., 2012; Cabedo-Sanz et al., 2013; Navarro-Rodriguez et al., 2013; Stoynova et al., 2013; Weckström et al., 2013; Xiao et al., 2013, 2015a, 2015b; Berben et al., 2014, 2017; Müller and Stein, 2014; Belt et al., 2015; Hoff et al., 2016; Polyak et al., 2016; Hörner et al., 2017; Pieńkowski et al., 2017). The adoption of a uniform scale (0–1) with the PIP_{25} index allows for more consistent comparisons of inferred sea ice conditions from different datasets, especially considering the variability of sedimentary IP_{25} concentration for regions of similar sea ice cover (Stoynova et al., 2013; Xiao et al., 2015a). However, several challenges are associated with sterol-based PIP_{25} indices. First, sterols are not particularly source-specific, being produced by a variety of marine and terrigenous sources (Volkman, 1986, 2006; Yunker et al., 2005; Rampen et al., 2010), including sympagic algae (Belt et al., 2013), which likely adds bias to PIP_{25} values in some settings. Second, a consequence of such ubiquity is a considerable discrepancy between the typical concentration ranges of sterols and IP_{25}, necessitating the use of a concentration balance factor, or *c*-factor, which can be adversely affected by, amongst other things, downcore concentration distributions and potential differential degradation of biomarkers in paleo-records (Belt and Müller, 2013).

To try and alleviate these limitations, Belt et al. (2015) compared the spatial distribution of IP_{25} in Barents Sea surface sediments to that of a tri-unsaturated HBI (III; Fig. 1) thought to be only biosynthesised by certain open-water diatoms belonging to the *Pleurosigma* and *Rhizosolenia* genera (Belt et al., 2000; Rowland et al., 2001) – including some species present in mixed phytoplankton communities from western Svalbard (Belt et al., 2017) – and thus likely to provide a more selective

representation of the pelagic environment than many other biomarkers. Since the contribution of *Pleurosigma* spp. and *Rhizosolenia* spp. to many pelagic diatom assemblages and the proportion of IP_{25}-producing sympagic diatoms in sea ice are generally similar (ca. 1–5%; von Quillfeldt, 2000; Ratkova and Wassmann, 2005; Brown et al., 2014b), it was also hypothesized that sedimentary concentration ranges of III and IP_{25} would be comparable. Consistent with this background, an inverse relationship between IP_{25} and III was found for regions of contrasting sea ice cover, while $P_{III}IP_{25}$ indices (i.e. PIP_{25} based on IP_{25} and III) exhibited a vastly reduced influence of the *c*-factor on downcore profiles compared to those of P_BIP_{25} (i.e. PIP_{25} based on IP_{25} and brassicasterol), due to similar sedimentary concentrations of IP_{25} and III, as predicted (Belt et al., 2015). Using the same dataset, Smik et al. (2016) demonstrated a positive linear correlation between $P_{III}IP_{25}$ and spring sea ice concentration (SpSIC), thus providing a regional calibration, which has since been used to obtain semi-quantitative SpSIC estimates in downcore records (Cabedo-Sanz and Belt, 2016; Berben et al., 2017). However, several challenges inherent to the PIP_{25} index persist. Objective selection of optimal biomarkers that best describe spring sea ice conditions remains problematic, while the broad PIP_{25} thresholds previously used to classify regions of variable sea ice conditions, ranging from open water (PIP_{25} <0.1) to extensive sea ice cover (PIP_{25} >0.75) have not been based on a reproducible classification procedure, but instead determined using approximate data ranges obtained via linear regression of PIP_{25} and SpSIC (Müller et al., 2011; Smik et al., 2016). The application of a robust statistical procedure for multivariate HBI analysis could conceivably address these challenges and validate (or otherwise) the PIP_{25} approach for reconstructing paleo sea ice conditions.

Computational data mining algorithms incorporate a variety of parametric and non-parametric methods for multivariate analysis to characterise and visualise data structure (for reviews, see Rokach and Maimon, 2005; Sammut and Webb, 2017). Parametric algorithms, including cluster and factor analyses (e.g. Reimann et al., 2002; Templ et al., 2008), make distributional assumptions, such as data normality. However, geochemical data are seldom normally distributed due to strong spatial dependence, presence of statistical outliers, and missing data (Reimann and Filzmoser, 2000). In contrast, non-parametric methods, such as classification trees (CTs), make no significant distributional assumptions and often allow for intuitive visual interpretation of implicit trends (Aitchison, 1986; Vayssières et al., 2000; Vermeesch, 2006), an attribute not generally shared by parametric methods (Bunge, 1963). In essence, CTs are an example of a non-parametric technique used to determine the outcome of a categorical target (dependent) variable based on decisions made on a multivariate set of descriptive (independent) variables (e.g. Breiman et al., 1984; Quinlan, 1986,1993). A detailed review of decision tree methods is available from various authors (Rokach and Maimon, 2005; Hastie et al., 2009; Sammut and Webb, 2017), and an overview of the CT approach and associated terminology is included as part of Electronic Annex 1.

The principal aim of the current investigation, therefore, was to ascertain whether a CT model based on the variable distribution of certain biomarkers in marine sediments from across the Barents Sea could be used to accurately classify the overlying sea ice conditions and thus provide a novel and potentially more reliable approach to paleo sea ice reconstruction. To address this aim, CT models were constructed using relative abundances of six HBI biomarkers (Fig. 1) in *ca.* 200 surface sediments spanning the Barents Sea and neighbouring regions (Fig. 2a). An

optimized CT model was then used to reconstruct sea ice conditions in four well-dated short sediment cores retrieved from sites of contrasting sea ice conditions within the study region, and for which observational sea ice records covering recent centuries were also available (Divine and Dick, 2006; Vare et al., 2010; Walsh et al., 2017). Finally, the CT model results were compared to SpSIC estimates obtained from regionally calibrated $P_{III}IP_{25}$ indices.

2. Regional setting

The Barents Sea is a marginal area of the Arctic Ocean and is both the largest and deepest among the Arctic continental shelf regions. Detailed overviews of Barents Sea oceanography can be found in Loeng (1991) and Loeng et al. (1997). Briefly, Barents Sea hydrography is characterised by three distinct water masses (Fig. 2b): northward inflow of warm and saline Atlantic Water (AW), fresher and colder Arctic Water (ArW) flowing southwest, and brackish coastal water topographically steered along the Norwegian coast by the Norwegian Coastal Current (NCC) (Sakshaug et al., 2009).

Ice formation in the Barents Sea begins in October, reaching maximum extent in March–April. The direct inflow of AW (Loeng et al., 1997; Besczynska-Möller et al., 2012; Smedsrud et al., 2013) profoundly affects seasonal sea ice variability (Sorteberg and Kvingedal, 2006), keeping the region almost entirely ice-free at the September minimum, while the western Spitsbergen margin remains largely ice-free throughout the year (Walczowski and Piechura, 2011). The boundary where AW and ArW meet, known as the Polar Front (PF), defines the maximum winter ice extent and that of the highly productive MIZ (e.g. Wassmann et al., 1999). The position of the PF in winter is relatively constant in the western and central

Barents Sea (Loeng and Drinkwater, 2007) such that the MIZ experiences relatively low inter-annual variability. Sea ice in the eastern Barents Sea ice experiences increased seasonal and inter-annual variability due to the mixing of ArW and the North Cape Current (NCaC) inflow of AW. Sea ice in the Barents Sea, overall, has decreased by >50% since the beginning of satellite monitoring in 1979 (Fetterer et al., 2016), and a negative trend since 1850 has also been reported (Divine and Dick, 2006). This retreat and the seasonal amplitude of sea ice extent are likely accelerated by a combination of increasing inflow and temperature of the NAC (Årthun et al., 2012) and various positive feedback mechanisms (e.g. Smedsrud et al., 2013).

3. Materials and methods

3.1 Surface sediment material

198 surface sediment sub-samples were taken from a range of multicores, box cores and gravity cores reflecting regions of variable sea ice cover (Fig. 2a). Most of the sediment material has been described elsewhere (Knies and Martinez, 2009; Navarro-Rodriguez et al., 2013; Belt et al., 2015; Smik et al., 2016). 55 samples described previously (Navarro-Rodriguez et al., 2013) and 96 further sediments from the MAREANO program (http://www.mareano.no; Thorsnes, 2009) were re-extracted using fresh material sub-sampled at the Geological Survey of Norway. These were supplemented by 47 surface sediments from other sources (Belt et al., 2015), including material collected during the Centre for Arctic Gas Hydrate, Environment, and Climate (CAGE; UiT–Arctic University of Norway) cruises 15-2 and 16-5 aboard the RV *Helmer Hanssen* in 2015 and 2016, respectively (n=10). Upon arrival, all samples were freeze-dried (0.001 mbar; -80°C; *ca.* 24h) and stored in plastic bags at -20°C to avoid HBI degradation. A depth interval of 0–1 cm was sampled for the

majority of the sediments (n=188), while variable depths ranging from 0–3 cm were only used for 10 samples. Detailed grain size distributions were not available for every sample, although published data from the MAREANO programme (Knies et al., 2006) for 73 sediments indicate that most samples from the central and northern Barents Sea included a variable (40–85%) mud fraction (summed silt and clay particles ≤63µm), while sediment coarsening was observed towards coastal areas along the northern and north-western Norwegian coast, where silt and clay fractions were as low as 5%. Sampling locations and biomarker data are available from PANGAEA (www.pangaea.de)

3.2 Downcore sediment material

Downcore data were obtained from four short sediment cores (Fig. 2a) described elsewhere (Vare et al., 2010; Cabedo-Sanz and Belt, 2016). Cores BASICC 1 (73.13°N, 25.63°W; 425 m water depth), BASICC 8 (77.98°N, 26.83°W; 136 m water depth), and BASICC 43 (72.54°N, 45.74°W; 285 m water depth), henceforth referred to as cores 1, 8, and 43, were recovered aboard the RV *Ivan Petrov* in August 2003 as part of the `Barents Sea Ice Edge in a Changing Climate` (BASICC) project (Cochrane et al., 2009). Previously reported grain-size distributions indicated high mud content for cores 1 and 8 (*ca.* 89% and 77% summed silt and clay fraction, respectively), while core 43 exhibited a higher proportion of sand (*ca.* 47%; Cochrane et al., 2009). The age models for all three cores have been described elsewhere (Vare et al., 2010) and span the last *ca.* 250–300 years. Core MSM5/5-712-1 (78.92°N, 6.77°W; 1490.5 m water depth), hereafter referred to as core 712, was collected in 2007 on board the RV *Maria S. Merian* during the MSM5/5 cruise, and was described previously (Spielhagen et al., 2011; Cabedo-

Sanz and Belt, 2016). The uppermost 7.5 cm of core 712 analysed herein consist of fine-grained mud, with a consistently low content (*ca.* 5±1%) of sediment coarser than 0.63 µm (Werner et al., 2011). The age model spans the last *ca*. 2000 years (Spielhagen et al., 2011). The cores were chosen to represent open water (core 1), as well as intermediate (cores 43, 712) and extensive (core 8) seasonal sea ice conditions, at least during recent centuries (Divine and Dick, 2006; Walsh et al., 2017). Sedimentation rates for cores 1, 8 and 43 ranged from 1.1–1.3 mm y^{-1}, and were considerably lower (0.18 mm y^{-1}) for core 712, resulting in respective temporal resolutions of *ca.* 8–9 years and 56 years per 1.0 cm horizon. Downcore biomarker data are available from PANGAEA (www.pangaea.de).

3.3 Analysis of HBI biomarkers

The extraction of HBI lipids (I–VI; Fig. 1) was carried out according to methods described previously (Belt et al., 2012; Cabedo-Sanz and Belt, 2015). Internal standard (9-octylheptadec-8-ene; 0.1 µg) was added to freeze-dried sediments (*ca.* 1.5–2.5 g), which were then extracted (×3) by ultrasonication using dichloromethane/methanol (2:1 v/v, 2 mL) to obtain Total Organic Extracts (TOEs). Solvent was evaporated from the TOEs (N_2 stream, 25°C) and elemental sulphur was removed as described by Cabedo-Sanz and Belt (2015). The non-polar fraction containing HBI lipids was collected using open column silica chromatography (ca. 1 g silica; 6–7 mL hexane; Belt et al., 2012). Hexane was partially evaporated from the HBI-containing fractions (N_2 stream, 25°C), leaving *ca.* 200–300 µL. Further purification of the extracts was carried out using Ag-ion column chromatography (Supelco Discovery® Ag-Ion; 0.12 g), separating the extracts into saturated hydrocarbons (1 mL hexane) and HBIs (2 mL acetone). Analysis of HBI-containing

fractions was carried out using gas chromatography–mass spectrometry (GC–MS) in total ion current (TIC) and single ion monitoring (SIM, *m/z* 346 (HBIs III–V), 348 (II and VI) and 350 (I)) modes using an Agilent 7890 series gas chromatograph (HP_{5MS} fused silica column; 30 m × 0.25 mm i.d., 0.25 µm film thickness) coupled to an Agilent 5975 mass spectrometric detector (Belt et al., 2012). HBIs were identified by comparison of retention indices ($RI_{HP5\text{-}MS}$) and mass spectra to those of authentic standards. Quantification of HBIs (ng g^{-1} dry sed.) was carried out by comparing mass spectral intensities of molecular ions to that of the internal standard, and normalising for differences in mass spectral fragmentation efficiency and sediment mass. Chromatographic data from sediment material described by Belt et al. (2015) were re-examined to quantify HBIs not measured previously.

3.4 Statistical procedure

3.4.1 Data preparation

SpSIC data (April–June, 1988–2007) were obtained from Nimbus-7 SMMR and DMSP SSM/I-SSMIS passive microwave datasets (Cavalieri et al., 1996). The same dataset was used previously for biomarker-based pan-Arctic and regional sea ice calibrations via the PIP_{25} index (Xiao et al., 2015a; Smik et al., 2016). Sediment sampling dates and regional accumulation rates supported the selection of an appropriate time interval covered by the satellite data. The majority of surface sediment material was collected from 2003–2006 (Navarro-Rodriguez et al., 2013; Belt et al., 2015), while Barents Sea sedimentation rates in ice-covered regions are typically 0.7±0.4 mm y^{-1} (e.g. Zaborska et al., 2008), but can reach 1.1±0.4 mm y^{-1} (Maiti et al., 2010). A 20-year time interval was therefore chosen for satellite-derived SpSIC to represent accumulation of 1.0 cm of sediment at 0.5 mm y^{-1}, the median of

the 0.2–0.8 mm y^{-1} range reported for the seasonal sea ice zone around Svalbard (Zaborska et al., 2008). $P_{III}IP_{25}$ indices were calculated using Eq. 1, with HBI III (defined as III in Eq. 1) as the pelagic biomarker counterpart to IP_{25}, and a regional *c*-factor (*c*=0.63) determined from a previous calibration (Smik et al., 2016). Square brackets denote absolute HBI concentrations (ng g^{-1} dry sed.) in all equations. Estimates of SpSIC (%) and associated standard errors were calculated using Eq. 2 and the root-mean-square error (RMSE) of the regional calibration, respectively (Cabedo-Sanz and Belt, 2016; Smik et al., 2016).

$$P_{III}IP_{25} = \frac{[IP_{25}]}{([IP_{25}] + [III] \times 0.63)} \#(1)$$

$$SpSIC\ (\%) = \frac{(P_{III}IP_{25} - 0.0692)}{0.0107} \#(2)$$

Prior to classification tree induction, the optimal number of classes representing different sea ice conditions was determined via complete linkage Agglomerative Hierarchical Clustering (AHC; Sørensen, 1948) of satellite-derived SpSIC estimates and coordinates of surface sediments (Fig. A.1, Electronic Annex 1). Squared Euclidean distance was used as a mathematical distance measure. Thus, three classes representing marginal (0–10%), intermediate (10–50%) and extensive (50–100%) SpSIC were identified (Fig. 3a). HBI concentrations were converted into relative abundances (0–100%) via separate normalisation to four HBI assemblages (Eq. 3).

$$HBI\ (\%) = \frac{[HBI]}{[HBI\ Assemblage]} \times 100\ \#(3)$$

The four HBI assemblages used for calculation of relative abundances are shown in Eq. 4–7. Biomarkers I–IV were included in all four assemblages (A to D) due to the likely contrasting influences of sea ice conditions on their production.

Thus, HBIs I (IP_{25}) and II have known sympagic diatom sources (Brown et al., 2014b; Belt et al., 2016), while III and IV are often co-produced in ubiquitous pelagic diatoms (Belt et al., 2000; Rowland et al., 2001). HBI IV has also been reported in sea ice (Belt et al., 2007; Brown, 2011; Ringrose, 2012). For Assemblage B, HBI V was also included as it has been identified in Arctic sea ice (Belt et al., 2007). An additional pelagic influence was investigated using VI (Assemblage C), an HBI reported in the diatom *Berkeleya rutilans*, a species abundant within (at least) brackish coastal waters (Brown et al., 2014a). The combined effect of V and VI on sea ice conditions was tested in Assemblage D.

$$HBI\ Assemblage\ A = \sum([I], [II], [III], [IV])\ \#(4)$$

$$HBI\ Assemblage\ B = \sum([I], [II], [III], [IV], [V])\ \#(5)$$

$$HBI\ Assemblage\ C = \sum([I], [II], [III], [IV], [VI])\ \#(6)$$

$$HBI\ Assemblage\ D = \sum([I], [II], [III], [IV], [V], [VI])\ \#(7)$$

3.4.2 Classification tree induction from sedimentary HBI composition

CT models were used to develop a predictive model for discrimination of discrete classes of sea ice cover (the target variable), using relative abundances of HBIs (descriptive variables). CT models were built from the surface sediment dataset following the method of Breiman et al. (1984). Specifically, the ‘rpart’ (Therneau et al., 2015), ‘caret’ (Kuhn et al., 2016), ‘rpartScore’ (Galimberti et al., 2012), ‘rpart.plot’ (Milborrow, 2017), ‘MLmetrics’ (Yan, 2016), ‘readr’ (Wickham et al., 2017), and ‘DMwR’ (Torgo, 2010) libraries were utilised as part of the R Statistical Package (R Core Team, 2017) for induction and performance evaluation of four CT models using

HBI assemblages A–D as descriptive variables (Eq. 3–7), and classes of sea ice cover assigned to each sample using satellite SpSIC data (Fig. 3a) as the target variable. First, fully-grown trees were induced using no stopping criteria and information gain (Quinlan, 1986) as the splitting criterion. Subsequently, cost-complexity pruning and the 1-SE rule were applied to each CT model to counter overfitting, reduce tree complexity and improve interpretability. To avoid positive bias in model performance due to class imbalance, precision and sensitivity metrics were calculated for each class of sea ice conditions (Electronic Annex 1). Precision represented the percentage of accurate predictions, while sensitivity indicated the proportion of correct classifications in the training set. The F-1 score was calculated as the weighted average of precision and sensitivity. Finally, Cohen's Kappa statistic was used to confirm that model accuracy was significantly better than that obtained by random chance, with values >0.80 indicating "excellent" classification performance (Landis and Koch, 1977). The HBI assemblage that best classified sea ice conditions was chosen based on the expected performance of each pruned tree on unseen data (i.e. new samples not used in model construction) using repeated 10-fold cross validation (n=5; Breiman et al., 1984), the variables selected for splitting rules, as well as model complexity and interpretability. The annotated R script used for tree induction and class prediction is available in Electronic Annex 2.

4. Results

4.1 Classification tree models

CT models created from HBI assemblages A–D are henceforth referred to as models A–D, respectively. Models A–D yielded a high classification rate for the training data, with 186–188 samples classified correctly (ca. 94–95%; Table 1; Fig.

3b). Similarly, comparably high accuracy was observed following repeated (n=5) 10-fold cross validation (92 ± 5–6%; Table 1). All models exhibited identical tree structure and low complexity (2 splits and 3 leaf nodes; Fig. A.2) following cost-complexity pruning via the 1-SE rule. In all cases, only IP_{25} and IV were used as primary splitting variables (Fig. 4 and A.2), and good separation of the three sea ice classes was achieved (Fig. 5). Biomarkers II and III were chosen by the models as surrogate split variables to substitute for IP_{25} and IV, respectively, for cases where either may not have been measured; however, there were no such cases in the current dataset. HBIs V and VI contributed little descriptive and predictive power to the model and exhibited low relative importance (Fig. 6). Upon examining performance for individual classes of sea ice conditions, the lowest sensitivity (73–79%) and precision (65–69%) were observed for samples with intermediate SpSIC. The loss of sensitivity corresponded to 4–7 samples being misclassified into both marginal (n=3–5) and extensive (n=2) sea ice classes. Similarly, precision suffered due to the misclassification of 7–10 samples from the marginal to the intermediate sea ice class. In contrast, locations with marginal and extensive SpSIC were correctly classified with higher confidence, exhibiting sensitivity values of 94–95% (marginal SpSIC) and 91–96% (extensive SpSIC), as well as corresponding precision values of 97–98% and 84–85%. Class-averaged performance of the models was also comparable, with sensitivity and precision ranges of 87–89% and 85–87%, respectively. The highest overall sensitivity of 89% was observed for model D, while model A was the most precise (87%). Overall, all trees showed comparable (high) performance and interpretability, with identical splitting variables (Table 1 and Fig. A.2).

355 *4.2 CT and $P_{III}IP_{25}$–based sea ice estimates for downcore records*

356 Due to the highly comparable cross-validated model performance (Table 1),
357 identical tree structure and split variables (Fig. 3a and A.2), and low relative
358 importance of biomarkers V and VI (Fig. 6), model A was chosen to predict discrete
359 sea ice conditions for cores 1, 8, 43 and 712 (Fig. 7). Within the time period
360 represented by the core sub-samples (*ca.* 1750 AD–present) and a 95% accuracy
361 confidence interval of 91–94%, all horizons from cores 43 and 712 were classified
362 into the intermediate sea ice class (10–50% SpSIC), while cores 1 and 8 were
363 characterised as having experienced marginal (<10%) and extensive (50–100%) sea
364 ice cover, respectively. $P_{III}IP_{25}$-based SpSIC estimates also showed that extensive
365 sea ice cover (84–85%) was inferred throughout core 8, while ice-free conditions
366 prevailed at the core 1 site (Fig. 7). In contrast, cores 43 and 712 were characterised
367 by intermediate and more variable SpSIC (13–30% and 29–41%, respectively).
368 Further, a gradual decline in SpSIC was apparent for core 43 after *ca.* 1900 AD and
369 core 712 after *ca.* 1850 AD (Vare et al., 2010; Cabedo-Sanz and Belt, 2016).

370

371 **5. Discussion**

372 *5.1 Rationalising CT model outcomes*

373 The identification of IP_{25} as a primary splitting variable in all CT models to
374 differentiate ice–covered and ice–free settings (Fig. 5) is consistent with its sympagic
375 source (Belt et al., 2007; Brown et al., 2014b). Additionally, locations characterised
376 by intermediate (extensive) sea ice cover were effectively classified using high (low)
377 contribution from the pelagic HBI biomarker IV (Fig. 5). Based on 10-fold cross
378 validation performance (Table 1), decision rules derived from IP_{25} and IV accounted
379 for most of the predictive power of models A–D, with no other HBI percentage

contributions used as primary split variables. Nonetheless, comparable importance of variables IP_{25}, II, III and IV was observed for all models (Fig. 6). The high importance of II and III was attributed to their use as surrogate split variables (Breiman et al., 1984) in case either IP_{25} or IV could not be measured, and is consistent with their sympagic and pelagic sources, respectively. Conversely, relatively negligible descriptive power was contributed by HBIs V and VI (Fig. 6). This is perhaps to be expected since the coastal pelagic diatom source of VI entails elevated abundances in brackish coastal areas, such as fjords (Brown et al., 2014a), while V has previously been in in sea ice (Belt et al., 2007) and in ice-free temperate regions (He et al., 2016), and is thus not especially environment-specific.

More specific classification outcomes predicted by the CT models can be rationalised through consideration of sea ice dynamics and their impacts on primary productivity during the spring and summer blooms. For example, locations that experience extensive SpSIC in our dataset are characterised by a bloom of sympagic algae within the sea ice itself, triggered primarily by the rapid increase of solar radiation and favourable light incidence angle in March–April (Strass et al., 1996; Signorini et al., 2009; Leu et al., 2011). In the Barents Sea, such blooms are likely supported by upwelling of nutrient-rich AW (Ivanov et al., 2012) and are dominated by diatoms (Wassmann et al., 1999), likely explaining the higher relative abundances of IP_{25} (Fig. 5), which accumulates mostly in March–April, at least in the Canadian Arctic (Brown et al., 2011). Conversely, the productivity of pelagic phytoplankton remains low during this time, and instead follows the highly stratified waters within 20–50 km of the receding ice edge during the ice melt season in May–July, starting approximately two months after the ice algal bloom (Signorini et al., 2009; Leu et al., 2011; Janout et al., 2016). However, although pelagic

phytoplankton productivity is also possible beneath dense sea ice cover and can be initiated by light penetration through leads and polynyas in the Barents Sea (Willmes and Heinemann, 2016), the highly-productive ice edge conditions do not reach north and east of Svalbard until *ca.* July–August (Fetterer et al., 2016). This shortens the pelagic bloom duration in these areas, prior to the October ice advance, and probably explains the low relative abundance of IV (Fig. 5). Similarly, high model performance for the marginal sea ice class attests to the source specificity of IP_{25}, which was absent at nearly all ice-free locations, and in relatively low abundance at locations with <10% SpSIC. Such source selectivity permitted the separation of most samples belonging to the marginal class with a single CT decision rule (Fig. 5). The high range of HBI IV relative abundance in this area (Fig. 5) reflects the regional productivity variability (e.g. Olsen et al., 2003; Signorini et al., 2009), including the well-known enhancement proximal to the stratified waters of the MIZ (Wassmann et al., 1999).

The majority of samples belonging to the intermediate SpSIC class were also correctly classified. In such settings, HBI composition, with lower relative contribution of IP_{25} compared to the extensive sea ice cover sites, is consistent with a short duration of the under-ice algal bloom before the onset of ice melt in May, whereupon the meltwater discharge triggers strong stratification of the upper water column and the initiation of an intense pelagic phytoplankton bloom (Janout et al., 2016) leading to increased IV (and III; Belt et al., 2015). Lower performance was observed for the MIZ west of Svalbard, however, an area at the boundary between marginal and intermediate SpSIC (Fig. 3b, 3c and Table 1). This is potentially attributable to the highly variable sea ice conditions that characterise the region. While the continental slope remains ice-free throughout the year due to the direct inflow of warm AW with

the WSC, sea ice is present on the shelf during winter due to the topographically-steered inflow of colder ArW with the ESC, resulting in a density gradient preventing significant AW intrusion to the shelf (Fig. 2b; Walczowski and Piechura, 2011). Similar conditions characterise Whalers Bay north of Svalbard, which is often ice-free, even in February (Ivanov et al., 2012). Such influence of contrasting water masses and sea ice regimes favours production of both sympagic and pelagic biomarkers (e.g. Søreide et al., 2013; Belt et al., 2015; Smik et al., 2016; Smik and Belt, 2017). Accordingly, our dataset shows high relative abundances of both IP_{25} and IV in western Svalbard locations (Fig. 5). Elevated abundance of IP_{25} may also result from allochthonous input from the Svalbard shelf (e.g. via ice rafting) to the relatively ice-free margin, as seen with some terrigenous organic matter (Knies et al., 2007; Knies and Martinez, 2009). Southward transport of drift ice from the Nansen Basin into the Barents Sea represent a further potential allochthonous source of sympagic material (Kwok et al., 2005).

Some misclassification, although less prominent, was also observed in the eastern part of the study region (Fig. 3c), potentially due to an increase in seasonal and annual sea ice variability in this area compared to the MIZ of the central Barents Sea. Thus, the oceanic fronts in the eastern Barents Sea are defined by separate salinity and temperature gradients due to considerable influence of AW inflow with the NCaC, resulting in higher sea ice variability (Oziel et al., 2016) with consequential influence on the balance between sympagic and pelagic production. In fact, the more frequent misclassification of samples located along the highly dynamic sea ice edge, more generally, is likely a result of spatial shifts in sympagic and pelagic productivity regimes, and underlines the difficulty in identifying and characterising the MIZ using geochemical biomarkers alone.

On the other hand, the use of different coring techniques, as well as variable sediment accumulation rates and diverse depositional settings observed in the Barents Sea (e.g. Boitsov et al., 2009; Knies and Martinez, 2009; Maiti et al., 2010) potentially represent additional sources of misclassification error in CT model output. For example, several surface sediments in the current dataset were collected via gravity coring, which is a potential cause of uppermost sediment distortion (Leonard, 1990). Additionally, integrated proxy signals from surface sediments correspond to variable timescales, which are potentially different from the 20 years covered by our database of satellite-derived SpSIC, at least in some locations. While sediment accumulation rates in the seasonal sea ice zone around Svalbard are typically 0.7±0.4 mm y^{-1} (Zaborska et al., 2008), they may reach up to 1.1±0.4 mm y^{-1} closer to the sea ice edge (Maiti et al., 2010), and are higher in fjords and areas of sediment erosion south of Spitsbergen (Boitsov et al., 2009). Thus, a sediment depth of 1.0 cm may represent *ca.* 5–30 years of deposition. Further, a low number of sediments in the current dataset (n=10) were sampled at variable depths (ranging from 1–3 cm). Thus, some surface sediment data described herein may not be equally representative of the 20-year satellite SpSIC record. In practice, achieving complete temporal comparability of surface sediment signals is problematic without detailed accumulation rates for all locations. Nevertheless, the distribution of certain individual HBIs (IP_{25} and III) in Barents Sea sediments has been shown previously to be broadly consistent with modern sea ice conditions (Navarro-Rodriguez et al., 2013; Belt et al., 2015; Smik et al., 2016).

5.2 Downcore class predictions and comparison to the PIP_{25}-based SpSIC estimates

Our downcore records represent regions of contrasting modern sea ice conditions. Site 8 has consistently experienced extensive SpSIC (ca. 80%) for the

last 300 years (at least), in stark contrast to site 1, which has been ice-free during this period (Divine and Dick, 2006; Vare et al., 2010). Site 43 is located in the south-eastern Barents Sea at the modern winter sea ice margin, while site 712, despite being located farther north, is influenced by direct northward inflow of warm Atlantic Water from the WSC and therefore also experiences low SpSIC. The downcore semi-quantitative SpSIC estimates derived from $P_{III}IP_{25}$ indices (Smik et al., 2016) reflected this variability of modern sea ice conditions, with high values for core 8, similarly low values for cores 43 and 712, and ice-free conditions inferred for core 1 (Fig. 7). Further, the decline in $P_{III}IP_{25}$-derived SpSIC estimates seen for cores 43 and 712 from *ca*. 1900 yr AD and 1850 yr AD, respectively (Vare et al., 2010; Cabedo-Sanz and Belt, 2016) is also consistent with observational sea ice records for the region (Divine and Dick, 2006; Walsh et al., 2017).

The downcore $P_{III}IP_{25}$-derived SpSIC estimates (Fig. 7) were also consistent with the marginal, intermediate and extensive sea ice classes obtained using CT model A (Fig. 3b–3c) and the other CT models (Fig. A4). However, due to the broader scale of sea ice classifications, CT model A did not capture the gradual decline of sea ice cover observed in the $P_{III}IP_{25}$-derived SpSIC record of cores 43 and 712 (Fig. 7). Despite this, the sea ice classes inferred for downcore records are entirely consistent with both the overlying sea ice conditions and the classification of surface sediments (Fig. 3b–3c), where model A correctly classified the majority of samples representing extensive sea ice conditions near east and north Svalbard, the highly-variable intermediate sea ice cover of the MIZ in the central Barents Sea, and the open water and marginal ice conditions south of ca. 75°N. However, both $P_{III}IP_{25}$- and CT-based methods somewhat overestimated the sea ice cover near site 712 (western Svalbard). Specifically, semi-quantitative SpSIC estimates for site 712

were higher relative to site 43, which experiences similarly low modern sea ice concentration, while model A misclassified the majority of surface sediments in close proximity to site 712 from marginal to the intermediate sea ice class (Fig. 3b–3c), probably due to the highly variable sea ice dynamics that characterise the west Svalbard margin, as outlined earlier. As such, on the basis of the data presented here, the $P_{III}IP_{25}$- and CT-based methods may be more suitable for regions (or downcore temporal windows) where sea ice conditions are more consistent in terms of seasonal or annual advance/retreat cycles, including areas of relatively stable winter maximum sea ice extent and PF position in the central Barents Sea (Loeng and Drinkwater, 2007).

5.3 General comparison between CT models and PIP_{25} methods

The suitability of CT models as a complementary approach to PIP_{25}-based methods for paleo-reconstruction of sea ice conditions is discussed briefly here and summarised in terms of an initial assessment of perceived advantages and potential limitations of both methods (Table 2). The principal advantage of the PIP_{25} approach is the ability, in some cases, to provide more precise SpSIC information and hence identify relatively subtle trends in temporal data as shown here for cores 43 and 712 (Fig. 7). However, as a univariate measure, PIP_{25} is dependent on the *c*-factor (Eq. 2), whose magnitude is sensitive to both the individual pelagic biomarker and its concentration range, which itself varies between regions and temporal windows within downcore records (e.g. Müller et al., 2011; Belt and Müller, 2013; Belt et al., 2015; Cabedo-Sanz and Belt, 2016). While the latter limitation has been circumvented to some extent in the Barents Sea by using a fixed value *c*-factor (Smik et al., 2016), objective choice of an appropriate pelagic biomarker in other Arctic regions potentially remains a challenge. Additionally, the value of the *c*-factor

for the Barents Sea (Smik et al., 2016) is unlikely to extend to other Arctic regions, given the large circum-Arctic variability of biomarker concentration ranges in regions of similar sea ice concentration (e.g. Stoynova et al., 2013; Xiao et al., 2015a). Further regional calibrations, potentially based on IP_{25} and HBI III, are needed before this aspect can be fully resolved.

In contrast, classification trees, while only able to provide discrete categorical output, automatically select descriptive variables most relevant to the classification (IP_{25} and IV in the current study; Fig. 4 and A.2), and do not use redundant variables (i.e. V and VI; Fig. 6). Further, CT models are not dependent on the *c*-factor due to their multivariate nature, and provide performance metrics that may be used to assign a confidence level to classification. In contrast, categorisation of sea ice conditions using PIP_{25} indices remain largely qualitative and subject to interpretive bias. Consequently, classification trees can potentially provide outcomes that are more compatible when making comparisons between downcore records located within a geographical region of the model training dataset, and offer intuitive visualisation of trends (Fig. 4a and 5) even when used with datasets containing statistical outliers or redundant variables (Breiman et al., 1984). In addition, classes of sea ice conditions may be assigned to new samples, such as those from downcore records described herein (Fig. 7), with a certain degree of mathematical certainty derived from model evaluation (Table 1).

CT models are not without limitations, however, some of which may be amplified by the data structure used in the current study. The conversion of absolute HBI concentrations to relative abundances (Eq. 3 to 7) was used to confine the data to a uniform scale and make classification of temporal data possible, since the data ranges of absolute HBI concentrations in downcore records may not be represented

in modern settings and are likely to exhibit a strong regional dependence (Belt and Müller, 2013; Stoynova et al., 2013; Xiao et al., 2015a). However, CT models based on compositional data can be less stable, since relatively small changes within the training data can significantly impact tree structure (e.g. Aluja-Banet and Nafria, 2003). As such, like with PIP_{25}, separate models should probably be constructed on a regional basis. Since the same limitations apply with missing data, it is recommended, therefore, that sea ice class predictions are only carried out for samples where all biomarker data have been recorded. The potentially lower stability of CT models when using compositional data (Aitchison, 1986; Aluja-Banet and Nafria, 2003) also highlights the importance of excluding variables that are redundant to the classification task, despite the capacity of classification trees for automatic variable selection (Breiman et al., 1984). In the current context, this was achieved by using different combinations of biomarkers with known sympagic or pelagic diatom sources (i.e. HBIs I–VI; Eq. 4–7) as classifiers of ice cover, subsequent exclusion of redundant variables (V and VI; Fig. 6), and selecting the simplest combination of HBIs (CT model A; Fig. 4) without compromising classification performance (Table 1). For the same reason, other biomarkers of lower source specificity, including sterols (e.g. Belt et al., 2015; Cabedo-Sanz and Belt, 2016), were excluded from the outset.

6. Conclusions

CT models based on the HBI biomarker content in surface sediments from the Barents Sea and neighbouring regions provide a useful proxy method for characterising Arctic sea ice conditions. Outcomes from four CT models constructed using different HBI assemblages revealed that the sea ice diatom biomarker IP_{25} and a pelagic HBI triene counterpart (IV) were the most appropriate variables used for

classification of sea ice conditions. Further sympagic (II) and pelagic (III) biomarkers were identified as surrogate variables should IP_{25} or IV data be unavailable in future samples. A cross-validated mean classification rate of >90% was obtained from all models. $P_{III}IP_{25}$-based estimates of SpSIC in four downcore records provided reasonable spatial and temporal agreement with known sea ice trends obtained from satellite and observational records, and with CT model outcomes. However, compared to the main Barents Sea sites, the agreement between the proxy and observational records was poorer for a core from the west Svalbard margin, and the qualitative predictions of broad-scale sea ice variability obtained from the CT model did not capture subtle trends of known sea ice decline over the last ca. 150 years that could be identified via the $P_{III}IP_{25}$ approach. Despite some potential limitations of the CT approach, the automatic selection of appropriate HBI biomarkers for description of sea ice conditions, the quantitative model assessment via performance metrics, and the insensitivity to the *c*-factor (PIP_{25}) and statistical outliers, make it a potentially useful tool for providing discrete categorical assessment of paleo sea ice conditions archived in marine sediment cores.

Acknowledgments

This work was partially supported by the University of Plymouth and the Research Council of Norway through its Centre of Excellence funding scheme for CAGE, project number 223259. We thank three anonymous reviewers for providing numerous thoughtful comments and suggestions that helped improve the focus and clarity of this manuscript.

Figure Legends

Figure 1. Structures of C_{25} Highly-Branched Isoprenoid (HBI) biomarkers utilised in the current study.

Figure 2. Maps of the Barents Sea showing the study region and sample locations. (a) The locations of surface sediments (black circles) and downcore records (black squares) evaluated in the current study. Cores are identified by white numbering; (b) A simplified representation of the surface currents carrying major water masses (NAC: North Atlantic Current; WSC: West Spitsbergen Current; NCaC: North Cape Current; ESC: East Spitsbergen Current; PC: Persey Current; NCC: Norwegian Coastal Current). The average position of spring sea ice extent (April–June, 1988–2007; Cavalieri et al., 1996) corresponding to a 15% SpSIC threshold is shown by solid black lines, while the sea ice edge corresponding to a 0% SpSIC threshold is shown by the dashed black line for map (a) only. Maps were produced using the Ocean Data View software package, version 4.7.10 (Schlitzer, 2017).

Figure 3. Maps showing the distribution of categorical sea ice concentration (SpSIC) classes in surface sediments: (a) Assigned using threshold SpSIC values from satellite data; (b) Classified using CT model A on the training dataset; (c) Classified by CT model A following 10-fold cross validation. Samples with marginal, intermediate, and extensive overlying SpSIC are shown by red, yellow, and green dots, respectively. For (b) and (c), white dots represent misclassified samples from CT model A. The average position of sea ice extent (15% SpSIC threshold) and sea ice edge (0% SpSIC threshold) for April–June (1988–2007; Cavalieri et al., 1996) are shown by solid and dashed black lines, respectively.

Figure 4. Pruned tree structure for CT model A showing two splitting rules, corresponding relative HBI abundance thresholds, and final SpSIC classes assigned to terminal (leaf) nodes. Sensitivity values for each class are also shown. Left and right branches represent cases where a splitting condition is true and false, respectively.

Figure 5. Scatter plot showing the distribution of surface sediments within the data space of CT model A. Classes of marginal, intermediate, and extensive sea ice conditions determined using satellite SpSIC data (Fig. 3a) are shown by red circles, yellow squares, and green triangles, respectively. The coloured regions represent areas within the data space classified by CT model A as marginal (red), intermediate (yellow), and extensive (green) sea ice conditions. The regions are separated by model-determined decision boundaries (annotated black lines), which show the chosen HBI biomarkers and corresponding relative abundance thresholds used for splitting rules. Misclassified samples are represented by diamond symbols and correspond mostly to sites from west Svalbard.

Figure 6. Relative variable importance for SpSIC classification. Only results for model D are shown, since models A–C did not use all six HBI biomarkers. Variable importance values are based on the summed reduction of the loss function calculated from the model splitting rules, and take surrogate variables into account (Breiman et al., 1984).

Figure 7. Comparison of $P_{III}IP_{25}$- and CT model-derived sea ice conditions from four dated short cores (cores 1, 8, 43 and 712) from the study region representing contrasting modern-day sea ice cover (Fig. 2). The magnitude of each data point (left-hand axis) corresponds to the $P_{III}IP_{25}$-derived SpSIC and associated standard

649 error estimates based on the regional calibration of Smik et al. (2016). The colours of
650 each data point indicate the CT model A predictions of marginal (red), intermediate
651 (yellow) and green (extensive) sea ice conditions (Fig. 3). Note the consistent
652 agreement between $P_{III}IP_{25}$-derived SpSIC (left-hand axis) and categorical CT
653 model-based sea ice classifications (right-hand axis). A period of SpSIC decline after
654 1850 is shown by the annotated arrow.

655

656

Tables

Table 1. Summary of performance metrics for classification tree (CT) models A–D. Abbreviations represent classes of sea ice conditions based on satellite SpSIC (Fig. 3a): MAR = marginal; INT = intermediate; EXT = extensive.

Model	Training Accuracy (%)	10-fold CV accuracy (%; n = 5)	Per-class sensitivity (%)			Mean sensitivity (%)	Per-class precision (%)			Mean precision (%)	F1 score	Kappa
			MAR	INT	EXT		MAR	INT	EXT			
A	94	92 ± 6	95	72	96	87 ± 11	97	69	85	87 ± 12	0.9 ± 0.1	0.8 ± 0.1
B	95	92 ± 5	94	73	94	87 ± 12	97	67	84	85 ± 12	0.9 ± 0.1	0.8 ± 0.1
C	94	92 ± 6	94	75	91	87 ± 12	97	65	84	87 ± 11	0.9 ± 0.1	0.8 ± 0.2
D	95	92 ± 6	94	79	94	89 ± 12	98	67	84	86 ± 12	0.9 ± 0.1	0.8 ± 0.1

663 Table 2. Summary of advantages and limitations of PIP_{25}- and CT-based methods

664 for estimating spring sea ice conditions.

Method	Advantages	Limitations	Selected references
PIP_{25}	Intuitive scale (0–1), transferable between study sites;	Calculation and interpretation can be problematic when IP_{25}=0 or both biomarkers absent;	Belt and Müller, 2013 Belt et al., 2015 Müller et al., 2011 Smik et al., 2016
	Provides semi-quantitative sea ice concentration estimates, including SpSIC (%) in some cases;	Univariate measure affected by regional and downcore variability of the *c*-factor;	
	Potentially able to capture subtle changes in sea ice conditions;	Objective selection of an appropriate pelagic biomarker can be challenging	
	Requires quantification of two variables only		
Classification Trees	Multivariate method that is not affected by *c*-factor variability;	Provides discrete qualitative SpSIC class predictions only;	Breiman et al., 1984 Quinlan, 1986, 1993
	Automatic selection of the most appropriate variables for classification;	Requires quantification of multiple variables;	
	Model performance on future samples can be quantitatively estimated	Model structure can be affected by small changes in the training data;	
		Relatively large datasets required for model training	

665

7. References

Aitchison, J. (1986) *The statistical analysis of compositional data*. Chapman & Hall, Ltd., London.

Aluja-Banet, T. and Nafria, E. (2003) Stability and scalability in decision trees. *Comput. Stat.* **18**, 505-520.

Årthun, M., Eldevik, T., Smedsrud, L.H., Skagseth, Ø. and Ingvaldsen, R.B. (2012) Quantifying the influence of Atlantic heat on Barents Sea ice variability and retreat. *J. Climate* **25**, 4736-4743.

Belt, S.T., Allard, W.G., Massé, G., Robert, J.-M. and Rowland, S.J. (2000) Highly branched isoprenoids (HBIs): Identification of the most common and abundant sedimentary isomers. *Geochim. Cosmochim. Acta* **64**, 3839-3851.

Belt, S.T., Brown, T.A., Ringrose, A.E., Cabedo-Sanz, P., Mundy, C.J., Gosselin, M. and Poulin, M. (2013) Quantitative measurement of the sea ice diatom biomarker IP_{25} and sterols in Arctic sea ice and underlying sediments: Further considerations for palaeo sea ice reconstruction. *Org. Geochem.* **62**, 33-45.

Belt, S.T., Brown, T.A., Rodriguez, A.N., Sanz, P.C., Tonkin, A. and Ingle, R. (2012) A reproducible method for the extraction, identification and quantification of the Arctic sea ice proxy IP_{25} from marine sediments. *Anal. Methods* **4**, 705-713.

Belt, S.T., Brown, T.A., Smik, L., Tatarek, A., Wiktor, J., Stowasser, G., Assmy, P., Allen, C.S. and Husum, K. (2017) Identification of C_{25} highly branched isoprenoid (HBI) alkenes in diatoms of the genus *Rhizosolenia* in polar and non-polar marine phytoplankton. *Org. Geochem.* **110**, 65-72.

Belt, S.T., Cabedo-Sanz, P., Smik, L., Navarro-Rodriguez, A., Berben, S.M.P., Knies, J. and Husum, K. (2015) Identification of paleo Arctic winter sea ice limits and the marginal ice zone: Optimised biomarker-based reconstructions of late Quaternary Arctic sea ice. *Earth Planet. Sci. Lett.* **431**, 127-139.

Belt, S.T., Massé, G., Rowland, S.J., Poulin, M., Michel, C. and LeBlanc, B. (2007) A novel chemical fossil of palaeo sea ice: IP_{25}. *Org. Geochem.* **38**, 16-27.

Belt, S.T., Massé, G., Vare, L.L., Rowland, S.J., Poulin, M., Sicre, M.-A., Sampei, M. and Fortier, L. (2008) Distinctive ^{13}C isotopic signature distinguishes a novel sea ice biomarker in Arctic sediments and sediment traps. *Mar. Chem.* **112**, 158-167.

Belt, S.T. and Müller, J. (2013) The Arctic sea ice biomarker IP_{25}: a review of current understanding, recommendations for future research and applications in palaeo sea ice reconstructions. *Quat. Sci. Rev.* **79**, 9-25.

Belt, S.T., Smik, L., Brown, T.A., Kim, J.H., Rowland, S.J., Allen, C.S., Gal, J.K., Shin, K.H., Lee, J.I. and Taylor, K.W.R. (2016) Source identification and distribution reveals the potential of the geochemical Antarctic sea ice proxy $IPSO_{25}$. *Nat. Commun.* **7**, 12655.

Berben, S.M.P., Husum, K., Cabedo-Sanz, P. and Belt, S.T. (2014) Holocene sub-centennial evolution of Atlantic Water inflow and sea ice distribution in the western Barents Sea. *Clim. Past* **10**, 181-198.

Berben, S.M.P., Husum, K., Navarro-Rodriguez, A., Belt, S.T. and Aagaard-Sørensen, S. (2017) Semi-quantitative reconstruction of early to late Holocene spring and summer sea ice conditions in the northern Barents Sea. *J. Quaternary Sci.* **32**, 587-603.

Beszczynska-Möller, A., Fahrbach, E., Schauer, U. and Hansen, E. (2012) Variability in Atlantic water temperature and transport at the entrance to the Arctic Ocean, 1997–2010. *ICES J. Mar. Sci.* **69**, 852-863.

Bitz, C.M., Gent, P.R., Woodgate, R.A., Holland, M.M. and Lindsay, R. (2006) The Influence of Sea Ice on Ocean Heat Uptake in Response to Increasing CO_2. *J. Climate* **19**, 2437-2450.

Boitsov, S., Jensen, H.K.B. and Klungsøyr, J. (2009) Natural background and anthropogenic inputs of polycyclic aromatic hydrocarbons (PAH) in sediments of South-Western Barents Sea. *Mar. Environ. Res.* **68**, 236-245.

Breiman, L., Friedman, J., Stone, C.J. and Olshen, R.A. (1984) *Classification and regression trees*. CRC press, New York.

Brown, T.A. (2011) Production and preservation of the Arctic sea ice diatom biomarker IP_{25}. Ph.D. thesis, Plymouth Univ.

Brown, T.A., Belt, S.T. and Cabedo-Sanz, P. (2014a) Identification of a novel di-unsaturated C_{25} highly branched isoprenoid in the marine tube-dwelling diatom Berkeleya rutilans. *Environ. Chem. Lett.* **12**, 455-460.

Brown, T.A., Belt, S.T., Philippe, B., Mundy, C.J., Massé, G., Poulin, M. and Gosselin, M. (2011) Temporal and vertical variations of lipid biomarkers during a bottom ice diatom bloom in the Canadian Beaufort Sea: Further evidence for the use of the IP_{25} biomarker as a proxy for spring Arctic sea ice. *Polar Biol.* **34**, 1857-1868.

Brown, T.A., Belt, S.T., Tatarek, A. and Mundy, C.J. (2014b) Source identification of the Arctic sea ice proxy IP_{25}. *Nat. Commun.* **5**, 4197.

Brown, T.A., Yurkowski, D.J., Ferguson, S.H., Alexander, C. and Belt, S.T. (2014) H-print: a new chemical fingerprinting approach for distinguishing primary production sources in Arctic ecosystems. *Environ. Chem. Lett.* **12**, 387-392.

736 Bunge, M. (1963) A general Black Box Theory. *Philos. Sci.* **30**, 346-358.

737 Cabedo-Sanz, P. and Belt, S.T. (2015) Identification and characterisation of a novel
738 mono-unsaturated highly branched isoprenoid (HBI) alkene in ancient Arctic
739 sediments. *Org. Geochem.* **81**, 34-39.

740 Cabedo-Sanz, P. and Belt, S.T. (2016) Seasonal sea ice variability in eastern Fram
741 Strait over the last 2000 years. *Arktos* **2**, 22.

742 Cabedo-Sanz, P., Belt, S.T., Knies, J. and Husum, K. (2013) Identification of
743 contrasting seasonal sea ice conditions during the Younger Dryas. *Quat. Sci. Rev.*
744 **79**, 74-86.

745 [dataset] Cavalieri, D.J., Parkinson, C.L., Gloersen, P. and Zwally, H.J. (1996) *Sea*
746 *ice concentrations from Nimbus-7 SMMR and DMSP SSM/I-SSMIS passive*
747 *microwave data*. ver. 1.1. NASA DAAC at the National Snow and Ice Data Center.
748 Boulder, Colorado. (url: http://dx.doi.org/10.5067/8GQ8LZQVL0VL) [Digital Media,
749 updated yearly].

750 Cochrane, S.K.J., Denisenko, S.G., Renaud, P.E., Emblow, C.S., Ambrose Jr, W.G.,
751 Ellingsen, I.H. and Skarðhamar, J. (2009) Benthic macrofauna and productivity
752 regimes in the Barents Sea — Ecological implications in a changing Arctic. *J. Sea*
753 *Res.* **61**, 222-233.

754 Derocher, A.E., Andersen, M., Wiig, O., Aars, J., Hansen, E. and Biuw, M. (2011)
755 Sea ice and polar bear den ecology at Hopen Island, Svalbard. *Mar. Ecol. Progr.*
756 *Ser.* **441**, 273-279.

757 de Vernal, A., Gersonde, R., Goosse, H., Seidenkrantz, M.-S. and Wolff, E.W. (2013)
758 Sea ice in the paleoclimate system: The challenge of reconstructing sea ice from
759 proxies – An introduction. *Quat. Sci. Rev.* **79**, 1-8.

760 Divine, D.V. and Dick, C. (2006) Historical variability of sea ice edge position in the
761 Nordic Seas. *J. Geophys. Res. Oceans* **111**, C01001.

762 Fahl, K. and Stein, R. (2012) Modern seasonal variability and deglacial/Holocene
763 change of central Arctic Ocean sea-ice cover: New insights from biomarker proxy
764 records. *Earth Planet. Sci. Lett.* **351–352**, 123-133.

765 [dataset] Fetterer, F., Knowles, K., Meier, W.N. and Savoie, M. (2016) *Sea Ice Index*.
766 ver. 2. NSIDC: National Snow and Ice Data Center. Boulder, Colorado. (url:
767 http://dx.doi.org/10.7265/N5736NV7) [Digital Media, updated daily].

768 Galimberti, G., Soffritti, G. and Di Maso, M. (2012) Classification trees for ordinal
769 responses in R: The rpartScore package. *J. Stat. Softw.* **46**, 1-25.

770 Hansen, J., Ruedy, R., Sato, M. and Lo, K. (2010) Global surface temperature
771 change. *Rev. Geophys.* **48**, Rg4004.

772 Hastie, T., Tibshirani, R. and Friedman, J. (2009) *The Elements of Statistical*
773 *Learning: Data mining, inference, and prediction, 2nd Edition*. Springer, New York.

774 Hoff, U., Rasmussen, T.L., Stein, R., Ezat, M.M. and Fahl, K. (2016) Sea ice and
775 millennial-scale climate variability in the Nordic Seas 90 kyr ago to present. *Nat.*
776 *Commun.* **7**, 12247.

777 Hörner, T., Stein, R. and Fahl, K. (2017) Evidence for Holocene centennial variability
778 in sea ice cover based on IP_{25} biomarker reconstruction in the southern Kara Sea
779 (Arctic Ocean). *Geo-Mar. Lett.*, doi: 10.1007/s00367-00017-00501-y.

780 Ivanov, V.V., Alexeev, V.A., Repina, I., Koldunov, N.V. and Smirnov, A. (2012)
781 Tracing Atlantic Water signature in the Arctic sea ice cover east of Svalbard. *Adv.*
782 *Meteorol.* **2012**, 201818.

783 Janout, M.A., Hölemann, J., Waite, A.M., Krumpen, T., von Appen, W.-J. and
784 Martynov, F. (2016) Sea-ice retreat controls timing of summer plankton blooms in the
785 Eastern Arctic Ocean. *Geophys. Res. Lett.* **43**, 12493-12501.

786 Kinnard, C., Zdanowicz, C.M., Fisher, D.A., Isaksson, E., de Vernal, A. and
787 Thompson, L.G. (2011) Reconstructed changes in Arctic sea ice over the past 1,450
788 years. *Nature* **479**, 509-512.

789 Knies, J., Brookes, S. and Schubert, C.J. (2007) Re-assessing the nitrogen signal in
790 continental margin sediments: New insights from the high northern latitudes. *Earth*
791 *Planet. Sci. Lett.* **253**, 471-484.

792 Knies, J., Cabedo-Sanz, P., Belt, S.T., Baranwal, S.F. and Rosell-Melé, A. (2014)
793 The emergence of modern sea ice cover in the Arctic Ocean. *Nat. Commun.* **5**, 5608.

794 Knies, J., Jensen, H.K.B., Finne, T.E., Lepland, A. and Saether, O.M. (2006)
795 Sediment composition and heavy metal distribution in Barents Sea surface samples:
796 results from Institute of Marine Research 2003 and 2004 cruises. NGU rapport
797 2006.067, Trondheim, Norway.

798 Knies, J. and Martinez, P. (2009) Organic matter sedimentation in the western
799 Barents Sea region: Terrestrial and marine contribution based on isotopic
800 composition and organic nitrogen content. *Nor. J. Geol.* **89**, 79-89.

801 Knies, J., Pathirana, I., Cabedo-Sanz, P., Banica, A., Fabian, K., Rasmussen, T.L.,
802 Forwick, M. and Belt, S.T. (2017) Sea-ice dynamics in an Arctic coastal polynya
803 during the past 6500 years. *Arktos* **3**, 1.

804 Kuhn, M., Wing, J., Weston, S., Williams, A., Keefer, C., Engelhardt, A., Cooper, T.,
805 Mayer, Z., Kenkel, B., R Core Team, Benesty, M., Lescarbeau, R., Ziem, A.,
806 Scrucca, L., Tang, Y., Candan, C. and Hunt, T. (2016) *Caret: Classification and*
807 *Regression Training.* ver. 6.0-73. (url: https://cran.r-project.org/package=caret).

808 Kwok, R., Maslowski, W. and Laxon, S.W. (2005) On large outflows of Arctic sea ice
809 into the Barents Sea. *Geophys. Res. Lett.* **32**, L22503.

810 Landis, J.R. and Koch, G.G. (1977) The measurement of observer agreement for
811 categorical data. *Biometrics* **33**, 159-174.

812 Leonard, E. (1990) An assessment of sediment loss and distortion at the top of short
813 gravity cores. *Sed. Geol.* **66**, 57-63.

814 Leu, E., Søreide, J.E., Hessen, D.O., Falk-Petersen, S. and Berge, J. (2011)
815 Consequences of changing sea-ice cover for primary and secondary producers in
816 the European Arctic shelf seas: Timing, quantity, and quality. *Progr. Oceanogr.* **90**,
817 18-32.

818 Loeng, H. (1991) Features of the physical oceanographic conditions of the Barents
819 Sea. *Polar Res.* **10**, 5-18.

820 Loeng, H. and Drinkwater, K. (2007) An overview of the ecosystems of the Barents
821 and Norwegian Seas and their response to climate variability. *Deep-Sea Res. Pt. II*
822 **54**, 2478-2500.

823 Loeng, H., Ozhigin, V. and Ådlandsvik, B. (1997) Water fluxes through the Barents
824 Sea. *ICES J. Mar. Sci.* **54**, 310-317.

825 Maiti, K., Carroll, J. and Benitez-Nelson, C.R. (2010) Sedimentation and particle
826 dynamics in the seasonal ice zone of the Barents Sea. *J. Mar. Syst.* **79**, 185-198.

827 Massé, G., Rowland, S.J., Sicre, M.-A., Jacob, J., Jansen, E. and Belt, S.T. (2008)
828 Abrupt climate changes for Iceland during the last millennium: Evidence from high
829 resolution sea ice reconstructions. *Earth Planet. Sci. Lett.* **269**, 565-569.

830 Méheust, M., Fahl, K. and Stein, R. (2013) Variability in modern sea surface
831 temperature, sea ice and terrigenous input in the sub-polar North Pacific and Bering
832 Sea: Reconstruction from biomarker data. *Org. Geochem.* **57**, 54-64.

833 Meier, W.N., Hovelsrud, G.K., van Oort, B.E.H., Key, J.R., Kovacs, K.M., Michel, C.,
834 Haas, C., Granskog, M.A., Gerland, S., Perovich, D.K., Makshtas, A. and Reist, J.D.
835 (2014) Arctic sea ice in transformation: A review of recent observed changes and
836 impacts on biology and human activity. *Rev. Geophys.* **52**, 185-217.

837 Milborrow, S. (2017) *rpart.plot: Plot 'rpart' models: An enhanced version of*
838 *'plot.rpart'.* ver. 2.1.2. (url: http://www.milbo.org/rpart-plot).

839 Müller, J., Masse, G., Stein, R. and Belt, S.T. (2009) Variability of sea-ice conditions
840 in the Fram Strait over the past 30,000 years. *Nat. Geosci.* **2**, 772-776.

841 Müller, J. and Stein, R. (2014) High-resolution record of late glacial and deglacial sea
842 ice changes in Fram Strait corroborates ice–ocean interactions during abrupt climate
843 shifts. *Earth Planet. Sci. Lett.* **403**, 446-455.

844 Müller, J., Wagner, A., Fahl, K., Stein, R., Prange, M. and Lohmann, G. (2011)
845 Towards quantitative sea ice reconstructions in the northern North Atlantic: A
846 combined biomarker and numerical modelling approach. *Earth Planet. Sci. Lett.* **306**,
847 137-148.

848 Müller, J., Werner, K., Stein, R., Fahl, K., Moros, M. and Jansen, E. (2012) Holocene
849 cooling culminates in sea ice oscillations in Fram Strait. *Quat. Sci. Rev.* **47**, 1-14.

850 Navarro-Rodriguez, A. (2014) Reconstruction of Recent Palaeo Sea Ice Conditions
851 in the Barents Sea. Ph.D. thesis, Plymouth Univ.

852 Navarro-Rodriguez, A., Belt, S.T., Knies, J. and Brown, T.A. (2013) Mapping recent
853 sea ice conditions in the Barents Sea using the proxy biomarker IP_{25}: Implications for
854 palaeo sea ice reconstructions. *Quat. Sci. Rev.* **79**, 26-39.

855 Olsen, A., Johannessen, T. and Rey, F. (2003) On the nature of the factors that
856 control spring bloom development at the entrance to the Barents Sea and their
857 interannual variability. *Sarsia* **88**, 379-393.

858 Oziel, L., Sirven, J., Gascard, J.-C. (2016) The Barents Sea frontal zones and water
859 masses variability (1980–2011). *Ocean Sci.* **12**, 169-184.

860 Perovich, D.K. and Polashenski, C. (2012) Albedo evolution of seasonal Arctic sea
861 ice. *Geophys. Res. Lett.* **39**, L08501.

862 Perovich, D.K. and Richter-Menge, J.A. (2009) Loss of sea ice in the Arctic. *Annu.*
863 *Rev. Mar. Sci.* **1**, 417-441.

864 Pieńkowski, A.J., Navpreet, K.G., Furze, M.F.A., Mugo, S.M., Marret, F. and
865 Perreaux, A. (2017) Arctic sea-ice proxies: Comparisons between biogeochemical
866 and micropalaeontological reconstructions in a sediment archive from Arctic Canada.
867 *The Holocene* **27**, 665-682.

868 Polyak, L., Belt, S.T., Cabedo-Sanz, P., Yamamoto, M. and Park, Y.-H. (2016)
869 Holocene sea-ice conditions and circulation at the Chukchi-Alaskan margin, Arctic
870 Ocean, inferred from biomarker proxies. *Holocene* **26**, 1810-1821.

871 Quinlan, J.R. (1986) Induction of decision trees. *Mach. Learn.* **1**, 81-106.

872 Quinlan, J.R. (1993) *C4.5: Programs for machine learning*. Morgan Kaufmann
873 Publishers Inc., San Mateo, California.

874 R Core Team (2017) *R: A Language and Environment for Statistical Computing.* R
875 Foundation for Statistical Computing, Vienna. (url: https://www.r-project.org).

876 Rampen, S.W., Abbas, B.A., Schouten, S. and Sinninghe Damste, J.S. (2010) A
877 comprehensive study of sterols in marine diatoms (*Bacillariophyta*): Implications for
878 their use as tracers for diatom productivity. *Limnol. Oceanogr.* **55**, 91-105.

879 Ratkova, T.N. and Wassmann, P. (2005) Sea ice algae in the White and Barent
880 seas: composition and origin. *Polar Res.* **24**, 95-110.

881 Reimann, C. and Filzmoser, P. (2000) Normal and lognormal data distribution in
882 geochemistry: Death of a myth. Consequences for the statistical treatment of
883 geochemical and environmental data. *Environ. Geol.* **39**, 1001-1014.

884 Reimann, C., Filzmoser, P. and Garrett, R.G. (2002) Factor analysis applied to
885 regional geochemical data: Problems and possibilities. *Appl. Geochem.* **17**, 185-206.

886 Ribeiro, S., Sejr, M.K., Limoges, A., Heikkilä, M., Andersen, T.J., Tallberg, P.,
887 Weckström, K., Husum, K., Forwick, M., Dalsgaard, T., Massé, G., Seidenkrantz, M.-
888 S. and Rysgaard, S. (2017) Sea ice and primary production proxies in surface
889 sediments from a High Arctic Greenland fjord: Spatial distribution and implications for
890 palaeoenvironmental studies. *Ambio* **46**, 106-118.

891 Ringrose, A.E. (2012) Temporal and vertical distributions of IP_{25} and other lipid
892 biomarkers in sea ice from Resolute Bay, Nunavut, Canada. M.Phil. thesis, Plymouth
893 Univ.

894 Rokach, L. and Maimon, O. (2005) Decision trees, In *Data Mining and Knowledge*
895 *Discovery Handbook* (eds. O. Maimon, L. Rokach). Springer, Boston,
896 Massachussets. pp. 165-192.

897 Rowland, S.J., Allard, W.G., Belt, S.T., Massé, G., Robert, J.M., Blackburn, S.,
898 Frampton, D., Revill, A.T. and Volkman, J.K. (2001) Factors influencing the
899 distributions of polyunsaturated terpenoids in the diatom, *Rhizosolenia setigera*.
900 *Phytochemistry* **58**, 717-728.

901 Sakshaug, E., Johnsen, G.H. and Kovacs, K.M. (2009) *Ecosystem Barents Sea*.
902 Tapir Academic Press, Trondheim.

903 Sammut, C. and Webb, G.I. (2017) *Encyclopedia of Machine Learning and Data*
904 *Mining, 2nd Edition*. Springer, New York.

905 Schlitzer, R. (2017) *Ocean Data View.* ver. 4.7.10. (url: http://odv.awi.de).

906 Smedsrud, L.H., Esau, I., Ingvaldsen, R.B., Eldevik, T., Haugan, P.M., Li, C., Lien,
907 V.S., Olsen, A., Omar, A.M., Otterå, O.H., Risebrobakken, B., Sandø, A.B.,
908 Semenov, V.A. and Sorokina, S.A. (2013) The role of the Barents Sea in the Arctic
909 climate system. *Rev. Geophys.* **51**, 415-449.

910 Signorini, S.R. and McClain, C.R. (2009) Environmental factors controlling the
911 Barents Sea spring-summer phytoplankton blooms. *Geophys. Res. Lett.* **36**, L10604.

912 Smik, L. and Belt, S.T. (2017) Distributions of the Arctic sea ice biomarker proxy IP_{25}
913 and two phytoplanktonic biomarkers in surface sediments from West Svalbard. *Org.*
914 *Geochem.* **105**, 39-41.

915 Smik, L., Cabedo-Sanz, P. and Belt, S.T. (2016) Semi-quantitative estimates of
916 paleo Arctic sea ice concentration based on source-specific highly branched
917 isoprenoid alkenes: A further development of the PIP_{25} index. *Org. Geochem.* **92**, 63-
918 69.

919 Søreide, J.E., Carroll, M.L., Hop, H., Ambrose Jr, W.G., Hegseth, E.N., Falk-
920 Petersen, S. (2013) Sympagic-pelagic-benthic coupling in Arctic and Atlantic waters
921 around Svalbard revealed by stable isotopic and fatty acid tracers. *Mar. Biol. Res.* **9**,
922 831-850.

923 Sørensen, T. (1948) A method of establishing groups of equal amplitude in plant
924 sociology based on similarity of species and its application to analyses of the
925 vegetation on Danish commons. *Biol. Skr.* **5**, 1-34.

926 Sorteberg, A. and Kvingedal, B. (2006) Atmospheric forcing on the Barents Sea
927 winter ice extent. *J. Climate* **19**, 4772-4784.

928 Spielhagen, R.F., Werner, K., Sørensen, S.A., Zamelczyk, K., Kandiano, E.S.,
929 Budéus, G., Husum, K., Marchitto, T.M. and Hald, M. (2011) Enhanced modern heat
930 transfer to the Arctic by warm Atlantic Water. *Science* **331**, 450-453.

931 Stein, R., Fahl, K., Schade, I., Manerung, A., Wassmuth, S., Niessen, F. and Nam,
932 S.-I. (2017) Holocene variability in sea ice cover, primary production, and Pacific-
933 Water inflow and climate change in the Chukchi and East Siberian Seas (Arctic
934 Ocean). *J. Quaternary Sci.* **32**, 362-379.

935 Stein, R., Fahl, K., Schreck, M., Knorr, G., Niessen, F., Forwick, M., Gebhardt, C.,
936 Jensen, L., Kaminski, M., Kopf, A., Matthiessen, J., Jokat, W. and Lohmann, G.
937 (2016) Evidence for ice-free summers in the late Miocene central Arctic Ocean. *Nat.*
938 *Commun.* **7**, 11148.

939 Strass, V.H. and Nöthigö E.-M. (1996) Seasonal shifts in ice edge phytoplankton
940 blooms in the Barents Sea related to the water column stability. *Polar Biol.* **16**, 409-
941 422.

942 Stoynova, V., Shanahan, T.M., Hughen, K.A. and de Vernal, A. (2013) Insights into
943 Circum-Arctic sea ice variability from molecular geochemistry. *Quat. Sci. Rev.* **79**,
944 63-73.

945 Stroeve, J.C., Serreze, M.C., Holland, M.M., Kay, J.E., Malanik, J. and Barrett, A.P.
946 (2012) The Arctic’s rapidly shrinking sea ice cover: a research synthesis. *Clim.*
947 *Chang.* **110**, 1005-1027.

948 Templ, M., Filzmoser, P. and Reimann, C. (2008) Cluster analysis applied to regional
949 geochemical data: Problems and possibilities. *Appl. Geochem.* **23**, 2198-2213.

950 Therneau, T., Atkinson, B. and Ripley, B. (2015) *Rpart: Recursive Partitioning and*
951 *Regression Trees.* ver. 4.1-10. (url: https://cran.r-project.org/package=rpart).

952 Thorsnes, T. (2009) MAREANO – An introduction. *Nor. J. Geol.* **89**, 3.

953 Torgo, L. (2010) *Data Mining with R, learning with case studies*. CRC Press, Boca
954 Raton, Florida.

955 Vancoppenolle, M., Meiners, K.M., Michel, C., Bopp, L., Brabant, F., Carnat, G.,
956 Delille, B., Lannuzel, D., Madec, G., Moreau, S., Tison, J.-L. and van der Merwe, P.
957 (2013) Role of sea ice in global biochemical cycles: emerging views and challenges.
958 *Quat. Sci. Rev.* **79**, 207-230.

959 Vare, L.L., Massé, G. and Belt, S.T. (2010) A biomarker-based reconstruction of sea
960 ice conditions for the Barents Sea in recent centuries. *Holocene* **20**, 637-643.

961 Vare, L.L., Massé, G., Gregory, T.R., Smart, C.W. and Belt, S.T. (2009) Sea ice
962 variations in the central Canadian Arctic Archipelago during the Holocene. *Quat. Sci.*
963 *Rev.* **28**, 1354-1366.

964 Vayssières, M.P., Plant, R.E. and Allen-Diaz, B.H. (2000) Classification trees: An
965 alternative non-parametric approach for predicting species distributions. *J. Veg. Sci.*
966 **11**, 679-694.

967 Vermeesch, P. (2006) Tectonic discrimination of basalts with classification trees.
968 *Geochim. Cosmochim. Acta* **70**, 1839-1848.

969 Volkman, J.K. (1986) A review of sterol markers for marine and terrigenous organic
970 matter. *Org. Geochem.* **9**, 83-99.

971 Volkman, J.K. (2006) Lipid markers for marine organic matter, In *Marine Organic*
972 *Matter: Biomarkers, Isotopes and DNA* (ed. J.K. Volkman). Springer, Berlin,
973 Heidelberg. pp. 27-70.

974 Von Quillfeldt, C.H. (2000) Common Diatom Species in Arctic Spring Blooms: Their
975 Distribution and Abundance. *Bot. Mar.* **43**, 499-516.

976 Walczowski, W. and Piechura, J. (2011) Influence of the West Spitsbergen Current
977 on the local climate. *Int. J. Climatol.* **31**, 1088-1093.

978 Walsh, J.E., Fetterer, F., Scott Stewart, J. and Chapman, W.L. (2017) A database for
979 depicting Arctic sea ice variations back to 1850. *Geogr. Rev.* **107**, 89-107.

980 Wassmann, P., Ratkova, T., Andreassen, I., Vernet, M., Pedersen, G. and Rey, F.
981 (1999) Spring bloom development in the Marginal Ice Zone and the Central Barents
982 Sea. *Mar. Ecol.* **20**, 321-346.

983 Weckström, K., Massé, G., Collins, L.G., Hanhijärvi, S., Bouloubassi, I., Sicre, M.-A.,
984 Seidenkrantz, M.-S., Schmidt, S., Andersen, T.J., Andersen, M.L., Hill, B. and
985 Kuijpers, A. (2013) Evaluation of the sea ice proxy IP_{25} against observational and
986 diatom proxy data in the SW Labrador Sea. *Quat. Sci. Rev.* **79**, 53-62.

987 Werner, K., Spielhagen, R.F., Bauch, D., Hass, H.C., Kandiano, E. and Zamelczyk,
988 K. (2011) Atlantic Water advection to the eastern Fram Strait — Multiproxy evidence
989 for late Holocene variability. *Palaeogeogr. Palaeoclimatol. Palaeoecol.* **308**, 264-276.

990 Wickham, H., Hester, J., Francois, R., R Core Team, RStudio Team, Jylänki, J. and
991 Jørgensen, M. (2017) *Read Rectangular Text Data.* ver. 1.1.0. (url:
992 http://readr.tidyverse.org, https://github.com/tidyverse/readr).

993 Willmes, S. and Heinemann, G. (2016) Sea-ice wintertime lead frequencies and
994 regional characteristics in the Arctic, 2003-2015. *Remote Sens.* **8**, 4.

995 Xiao, X., Fahl, K., Müller, J. and Stein, R. (2015a) Sea-ice distribution in the modern
996 Arctic Ocean: Biomarker records from trans-Arctic Ocean surface sediments.
997 *Geochim. Cosmochim. Acta* **155**, 16-29.

998 Xiao, X., Fahl, K. and Stein, R. (2013) Biomarker distributions in surface sediments
999 from the Kara and Laptev seas (Arctic Ocean): Indicators for organic-carbon sources
1000 and sea-ice coverage. *Quat. Sci. Rev.* **79**, 40-52.

1001 Xiao, X., Stein, R. and Fahl, K. (2015b) MIS 3 to MIS 1 temporal and LGM spatial
1002 variability in Arctic Ocean sea ice cover: Reconstruction from biomarkers.
1003 *Paleoceanography* **30**, 969-983.

Yan, Y. (2016) *Machine Learning Evaluation Metrics.* ver. 1.1.1. (url: http://github.com/yanyachen/MLmetrics).

Yunker, M.B., Belicka, L.L., Harvey, H.R. and Macdonald, R.W. (2005) Tracing the inputs and fate of marine and terrigenous organic matter in Arctic Ocean sediments: A multivariate analysis of lipid biomarkers. *Deep-Sea Res. Pt. II* **52**, 3478-3508.

Zaborska, A., Carroll, J., Papucci, C., Torricelli, L., Carroll, M.L., Walkusz-Miotk, J. and Pempkowiak, J. (2008) Recent sediment accumulation rates for the Western margin of the Barents Sea. *Deep-Sea Res. Pt. II* **55**, 2352-2360.

Figure

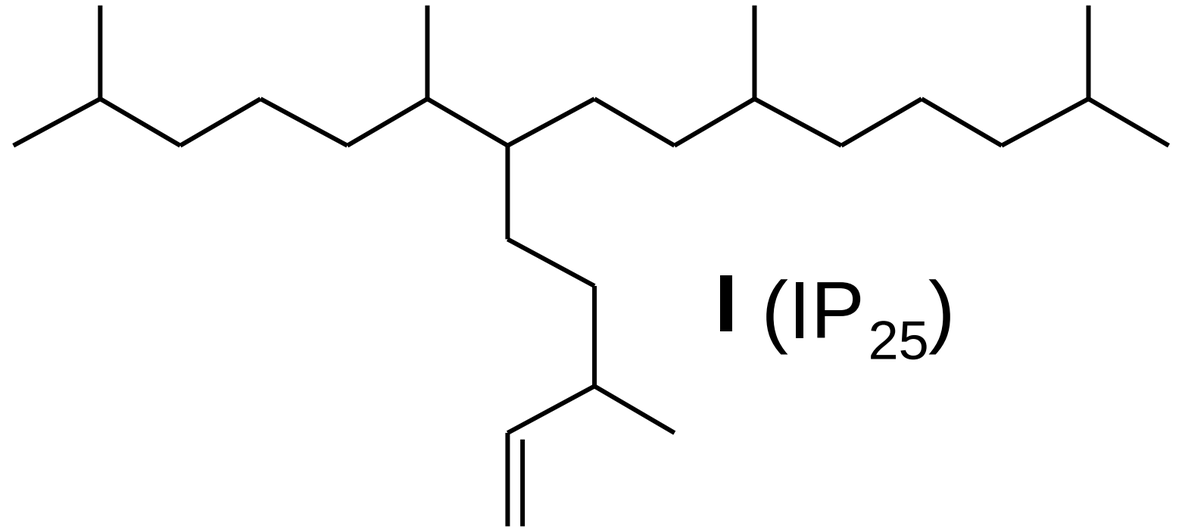

I (IP_{25})

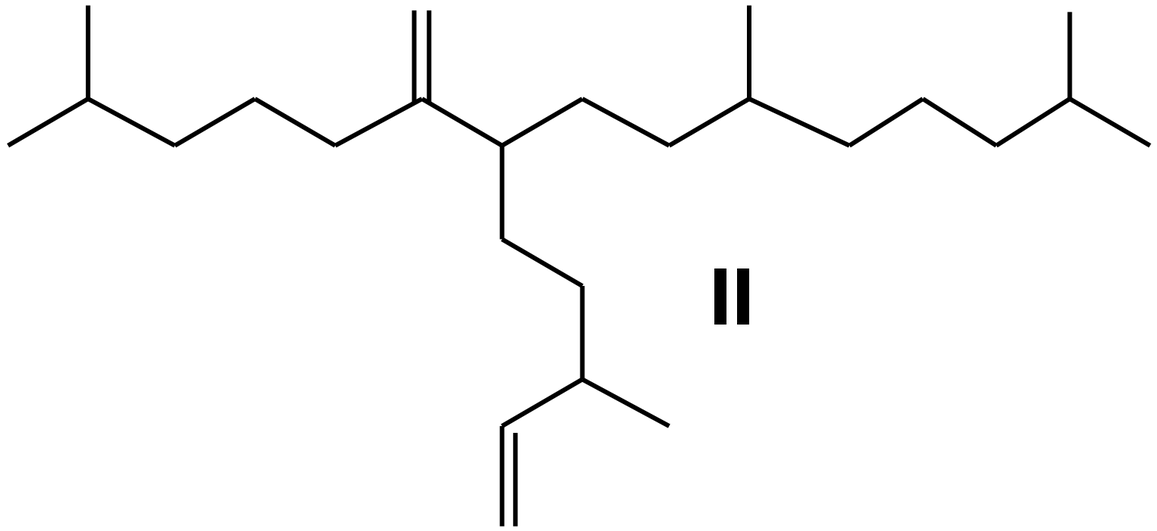

II

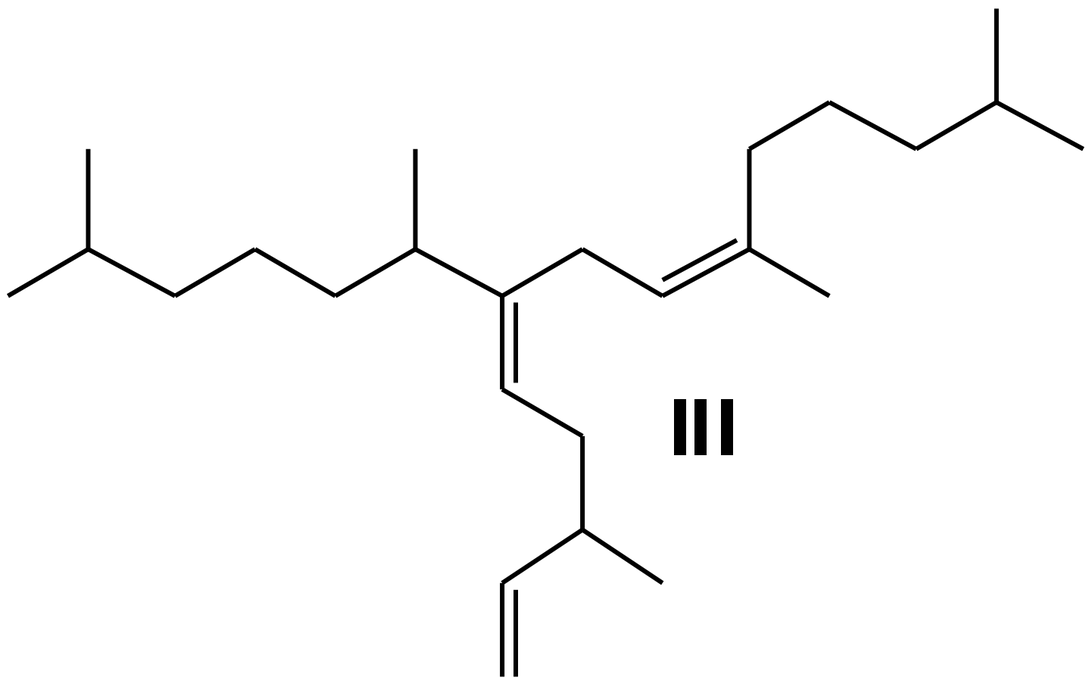

III

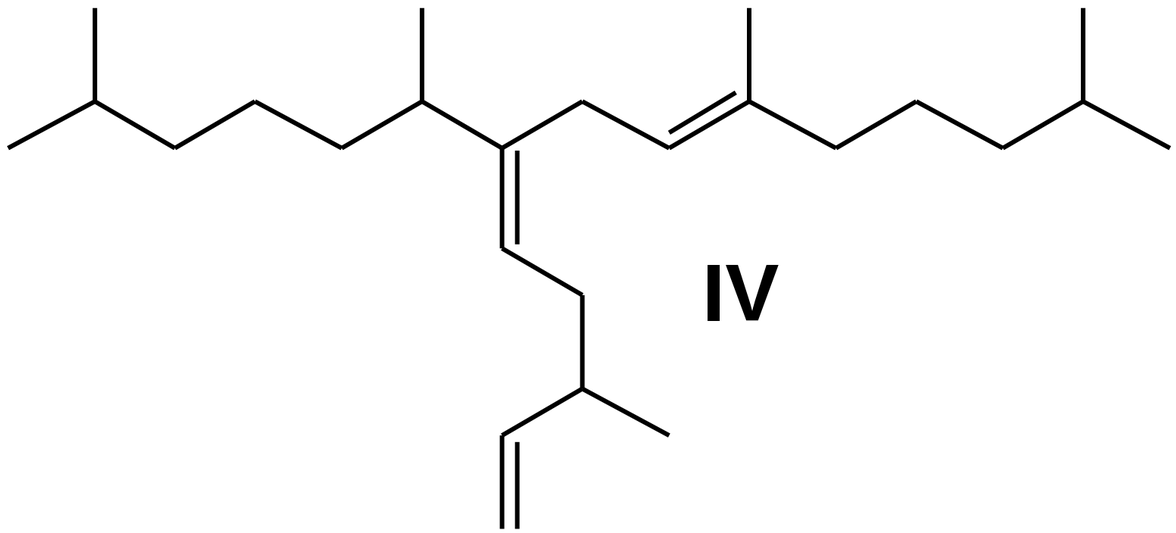

IV

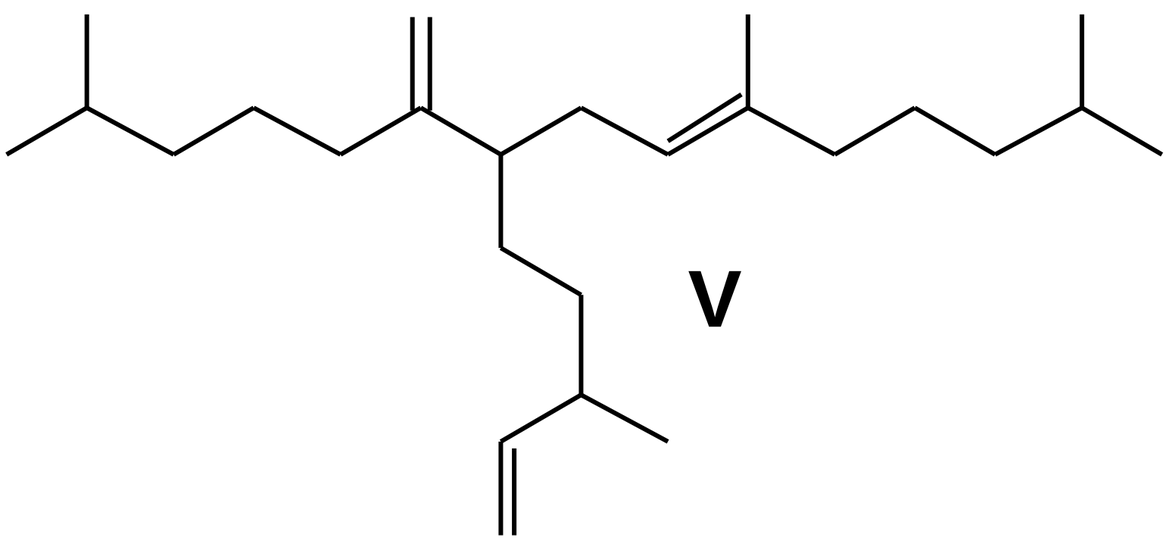

V

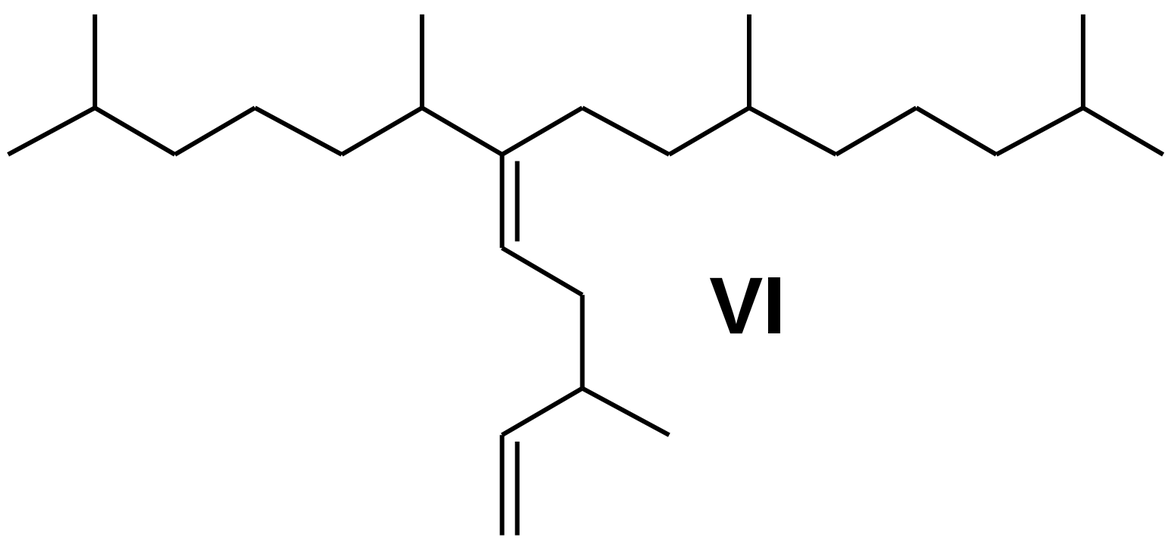

VI

Figure

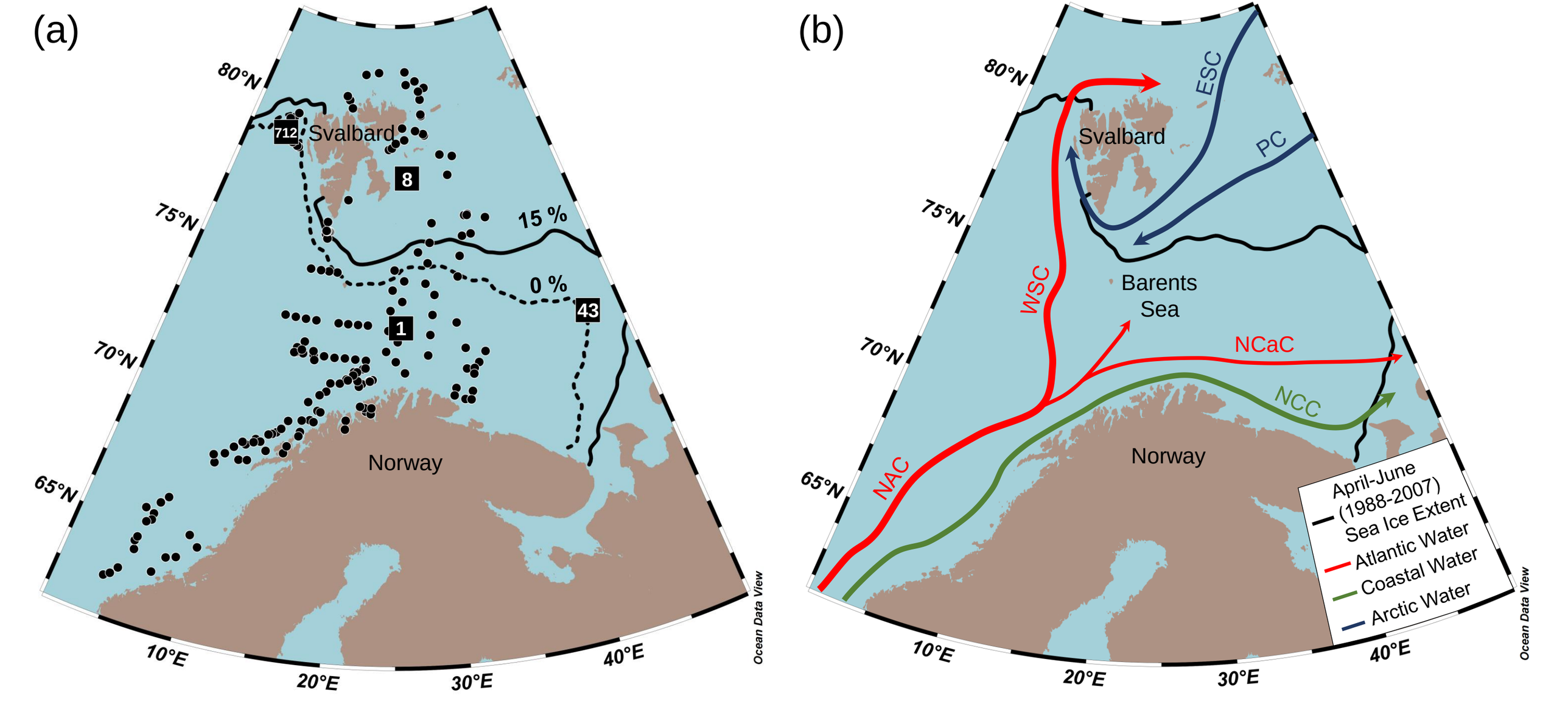

Figure

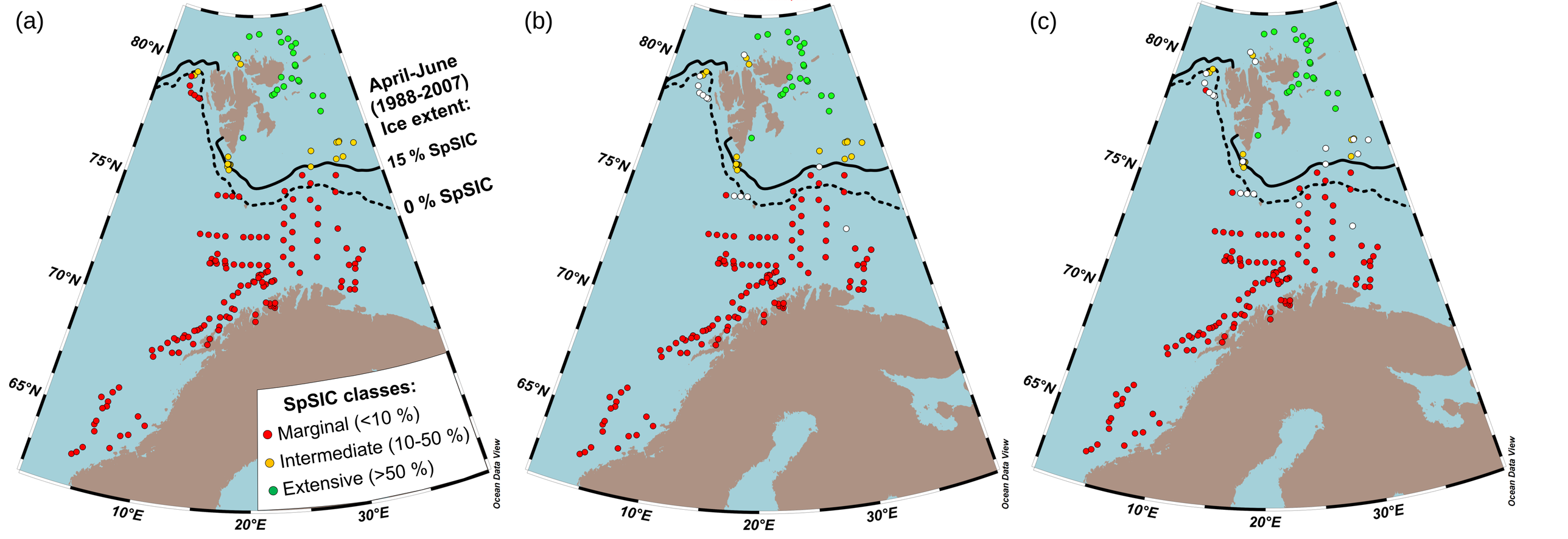

Figure

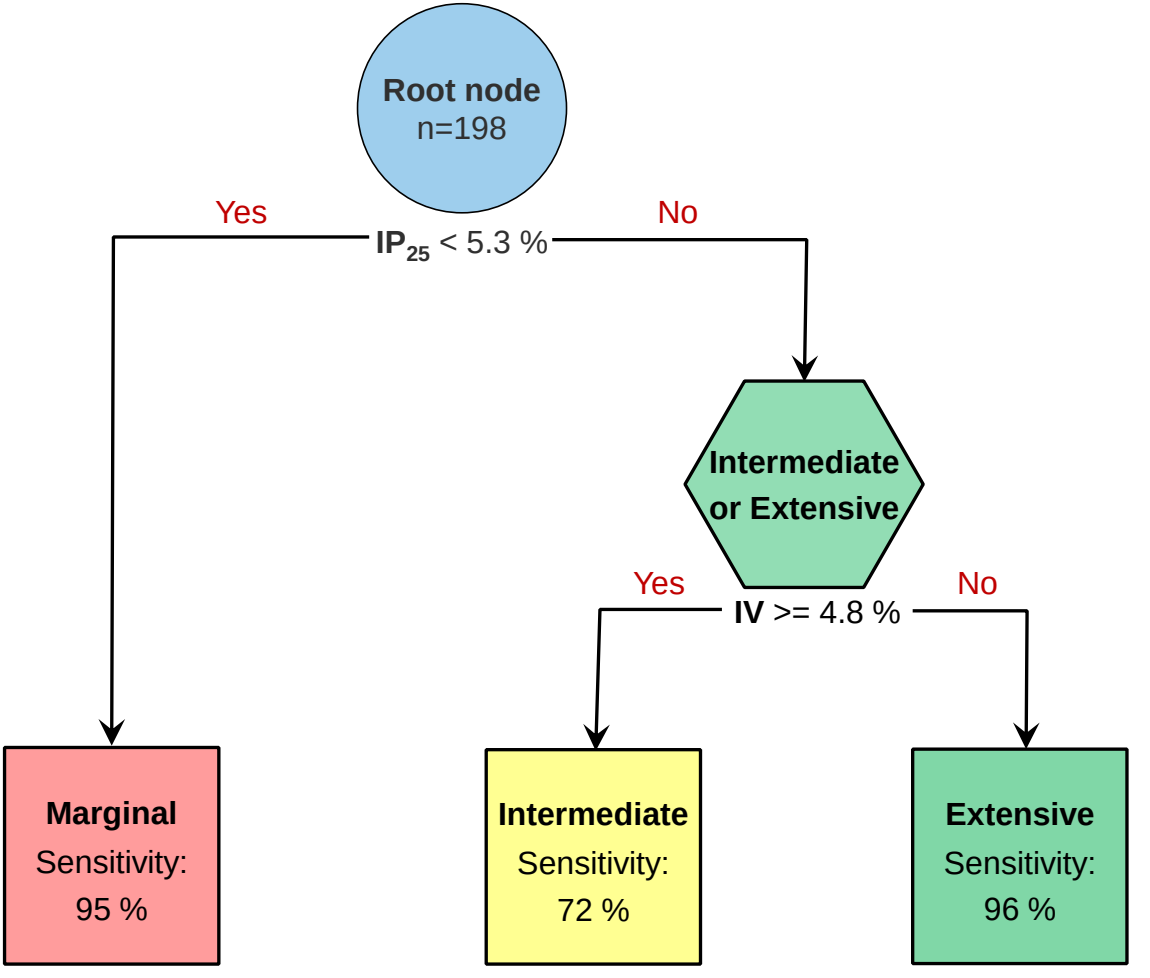

Figure

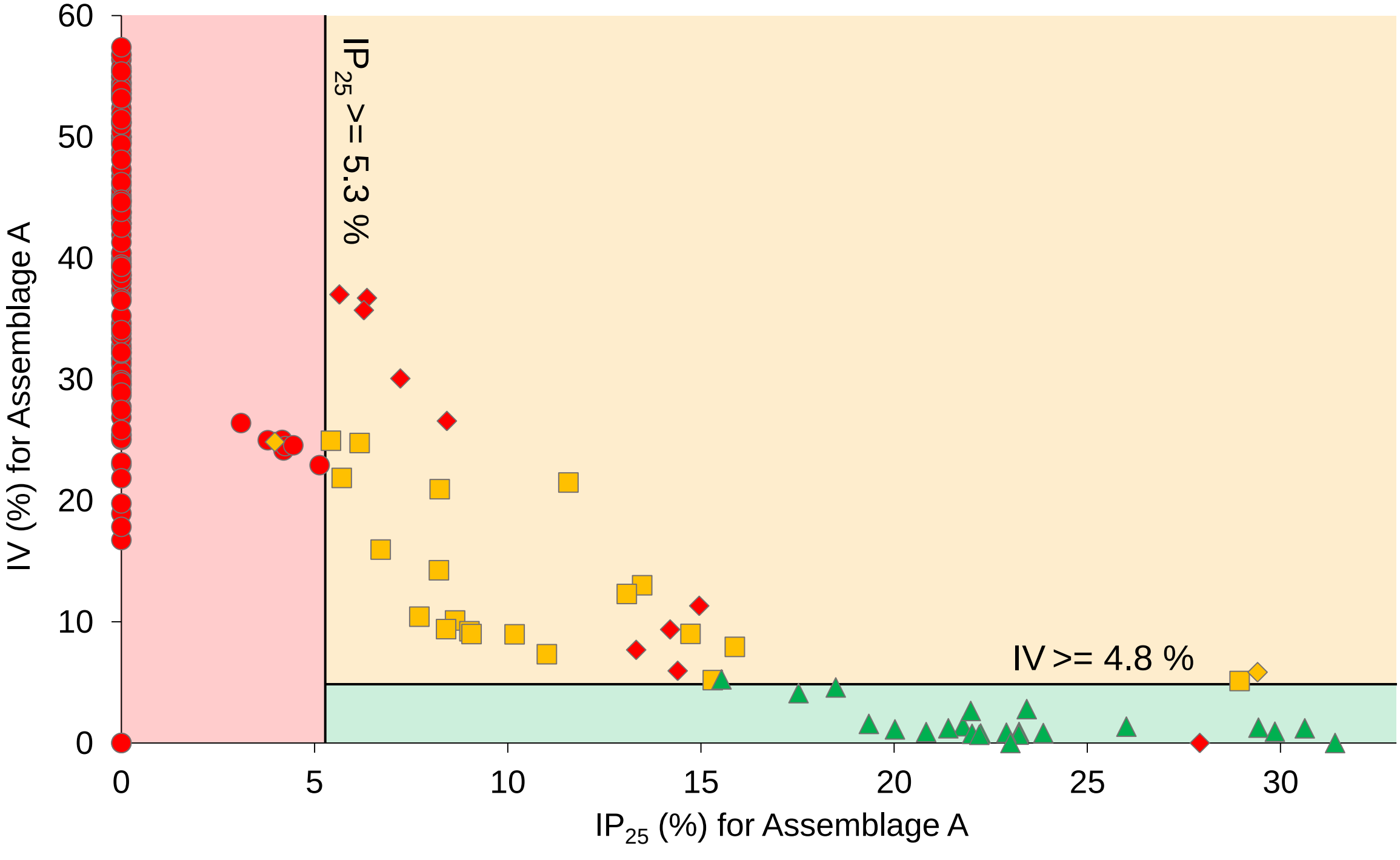

Figure

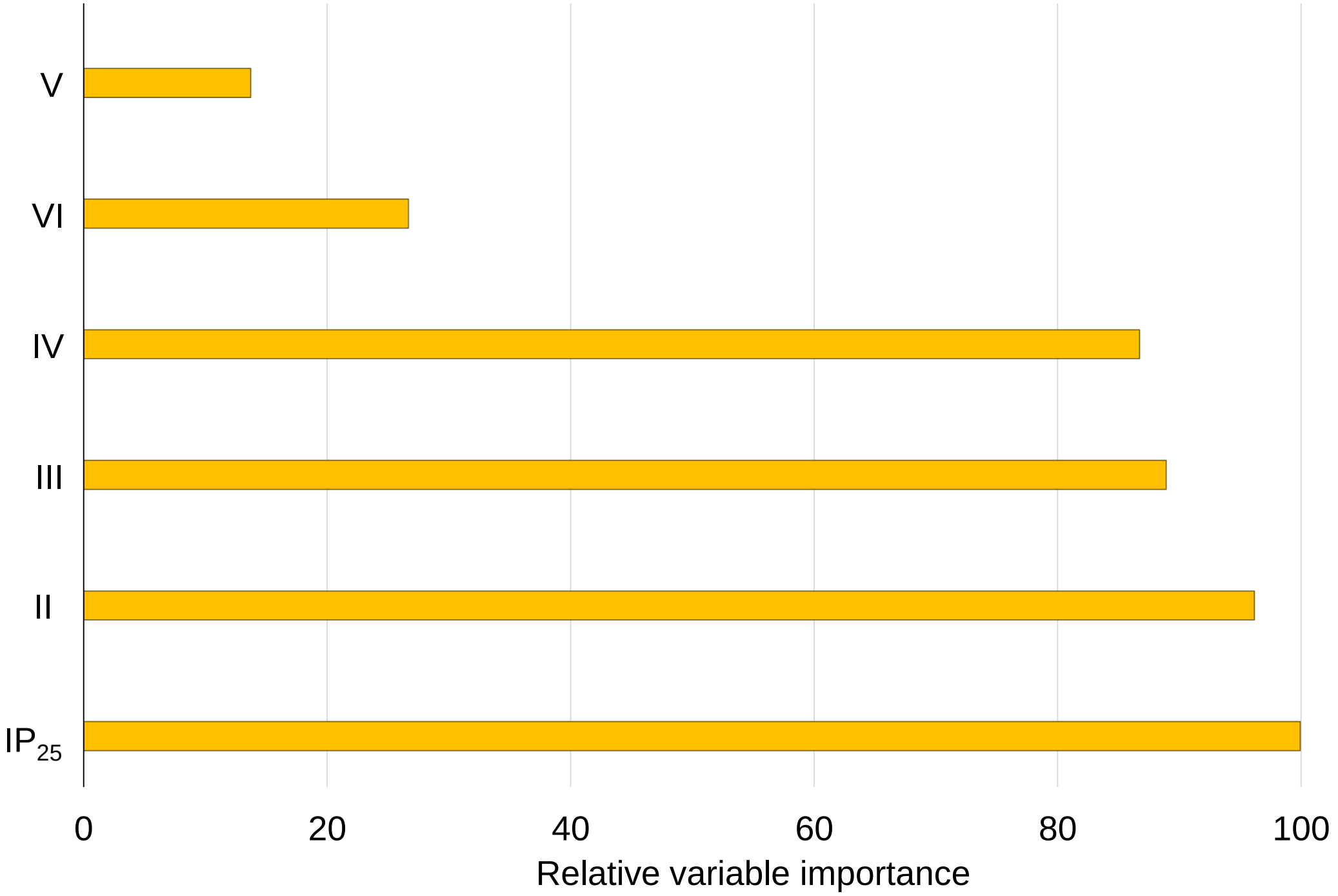

Figure

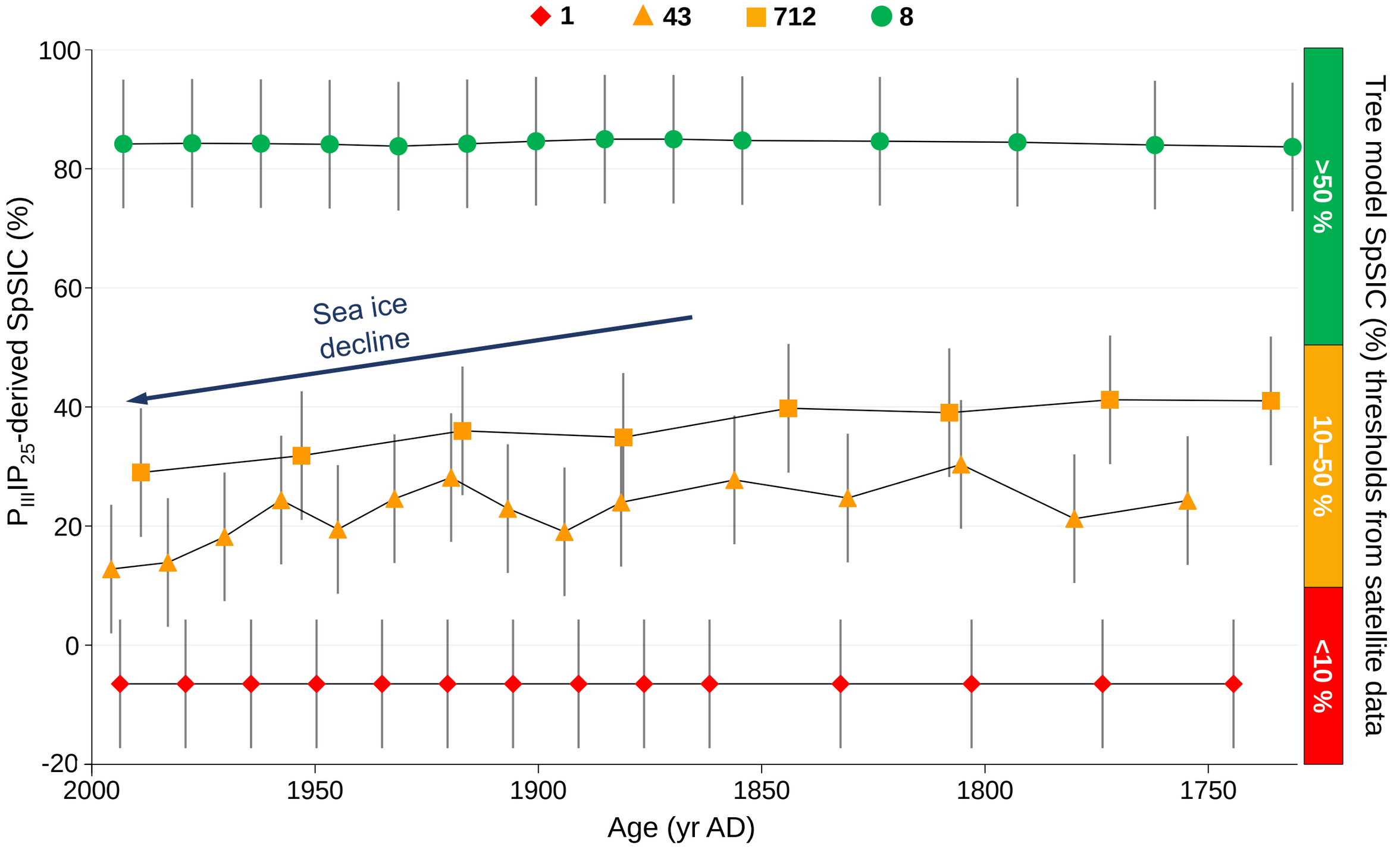

Electronic Annex

Click here to download Electronic Annex: Koseoglu et al_GCA_Electronic Annex 1_REVISED.pdf

Electronic Annex

Click here to download Electronic Annex: Koseoglu et al_GCA_Electronic Annex 2_REVISED.R